LITERATURE REVIEW

2.1 Introduction

Polymers are produced and used throughout the world because of their low cost, processing ease, and performance characteristics. Among these polymers, two that are greatly utilized are polyethylene (PE) and isotactic polypropylene (iPP). Commercially, microporous films of either PE or iPP, produced via the melt-extrusion/annealing/uniaxial-stretching method (MEAUS), are available and published research regarding these films exists.[1-4] Microporous polymeric membranes are generally composed of a continuous polymer matrix with pore sizes ranging from 0.001μm to 10μm where the micropores are evenly distributed within the film. Besides PE and iPP, comparatively little work exists concerning other microporous semicrystalline materials produced by what will be denoted in this proposal as the "uniaxial-stretching process". Specifically, no published work on isotactic poly(4-methyl-1-pentene) (PMP) microporous films has been presented. Microporous hollow fibers of PMP have been addressed in Japanese patent work[5] and a published report[6]. In addition, processing studies utilizing PMP almost solely deal with solid state extrusion[7,8] or fiber spinning.[9]

Polyethers are another group of polymers that are of commercial value, an example is polyoxymethylene (POM). The semicrystalline polymer POM has received attention in single crystal, crystallization, deformation, and processing studies.[10] A great deal of POM processing research has focused on such topics as solid state extrusion[11], various drawing schemes[12,13], and blown film crystallization studies[10,14]. Neither PMP or POM has been investigated as to the influences of the processing conditions on microporous film preparation via the uniaxial-stretching method. In addition, there is a lack understanding regarding which semicrystalline polymers can be processed into a "quality" microporous films, using the MEAUS process. Thus, it is not expected that there would be a set of "prerequisites" in selecting a polymer for this process of microporous film formation. However, before delving into the specifics of the

MEAUS process, some general information regarding uses for microporous membranes will be given followed by descriptions of microporous production methods. The background information on other microporous techniques will aid the reader in appreciating the elegance and importance (environmental and economic) of the MEAUS process relative to these other methods.

Polymeric microporous films are advantageous in comparison to ceramic and other microporous materials due to the ease of processing, cost, and performance characteristics. Films possessing a uniform concentration of micropores have a wide variety of applications. Six such applications are the following:

1) Microfiltration uses porous membranes where the micropores range in size from 0.1 to 10μm, and ultrafiltration where pores range from 1-10nm.
2) Gas separation in which either a homogeneous (non-porous) or microporous membrane is used.
3) Reverse osmosis is utilized in the separation of salt and microparticles.
4) Electrodialysis is an application in which the microporous polymer membrane is employed to desalt an ionic solution. The membranes for electrodialysis are typically cation or anion exchanging membranes.[15]
5) "Sensor"/"fail-safe" mechanism in which the microporous polymer membrane acts as a shutdown mechanism for a run-away exothermic chemical reaction.[15] An example of a "sensor"/"fail-safe" mechanism is as a separator in a Li-ion battery.

In this latter case, the microporous polymer membrane is a separator that insulates the electrodes of the battery. During discharge of the battery, electrons flow from the anode to the cathode through a motor or device requiring electricity. An electrolyte completes the circuit within the battery by furnishing ions from cathode to anode where the transfer of ions results in

an exothermic reaction. If this exothermic reaction should become thermally unstable, a runaway reaction results. In this case, the polymeric membrane will melt when the reaction temperature becomes greater than the melting point of the semicrystalline polymeric membrane. Upon melting, the micropores close, yet the membrane maintains its integrity thereby halting the reaction. If such a "fail-safe" mechanism were not in place, the battery could possibly explode or at least ruin the device to which it is supplying electricity.

The production of microporous membranes includes phase inversion[15-20], irradiation with subsequent etching[21-24], additive extraction[15], and methods utilizing stretching including the MEAUS process. A brief synopsis of each method is now given followed by a more in-depth discussion of the specific process studied in this research project (i.e. MEAUS method). The first method discussed is the phase inversion process. This process uses a polymer solution or "dope" that is cast into a film by contacting the solution with a non-solvent. The result is polymer coagulation from the solvent whereby a microporous membrane is formed under the proper conditions. Phase separation (i.e. coagulation) is achieved by contacting the "dope" with the high-boiling point non-solvent, and upon the application of heat the "good' solvent evaporates.[25] This method for microporous film production has been found to be applicable to cellulose, cellulose acetate, aromatic polyamides, polyacrylonitrile, poly(methyl methacrylate), and polysulfone polymers.[25] A problem with the phase inversion process is that solvents must be used which then incurs both financial and environmental costs (solvent recovery) to the manufacturer.

A second method of producing microporous film is the etching process of which there are basically two types. The first is extraction which initially requires mixing a polymer with a pore-forming agent such as a fine powder of a different polymer(s) to obtain a bicontinuous micro-phase separated system. The dispersed phase is subsequently removed by a solvent thereby creating a interconnected microporous morphology where the micropore distribution has been

found to greatly depend on starting film morphology.[26] The second etching method is termed "track-etching".[24] In tracking-etching, particles emanating from a nuclear reactor are passed through the film leaving tracks of degraded (not crosslinked) material. Following the tack-formation step, the film is then placed in an etching bath where the irradiated/degraded material is removed thus creating very uniform cylindrical micropores where the micropore diameter is controlled by the residence time in the etching bath.

In addition to the above processes, there are three micropore formation methods that require a stretching stage. The first, denoted here as solvent swelling, uses a semicrystalline polymer which is contacted with a swelling agent thereby preferentially swelling the amorphous regions. The swelled system is uniaxially[27] or biaxially[28] stretched where the crystalline phase then acts as a physical crosslink. Finally while the film is still in its stretched state, the swelling-agent is removed thereby leaving a microporous morphology. The second stretching method is unique because of the addition of a hard particulate filler, such as $CaCO_3$, during melt-extrusion. Uniaxial or biaxial stretching then follows where the hard particles act as stress concentrators in their vicinity thus aiding in the creation of the micropores.[29-31] For this method or any method utilizing particles to produce micropores, poor adhesion or wetting of the particles by the polymer must occur to generate micropores.

The final stretching method is the MEAUS process, which utilizes only semicrystalline polymeric materials. In this process, the initial step is melt-extrusion of the polymer into a film (precursor), followed by annealing, and subsequently uniaxial stretching along the machine direction (MD) of the film. As discussed in the literature, upon melt-extrusion, the resulting lamellar morphology has been observed to be influenced by the level of stress applied to the molten polymer during extrusion. "High" extrusion stress levels produce planar stacked lamellar morphologies, whereas "low" stress conditions produce a more twisted row-nucleated morphology.[32] This qualitative description is shown schematically in Figure 2.1.

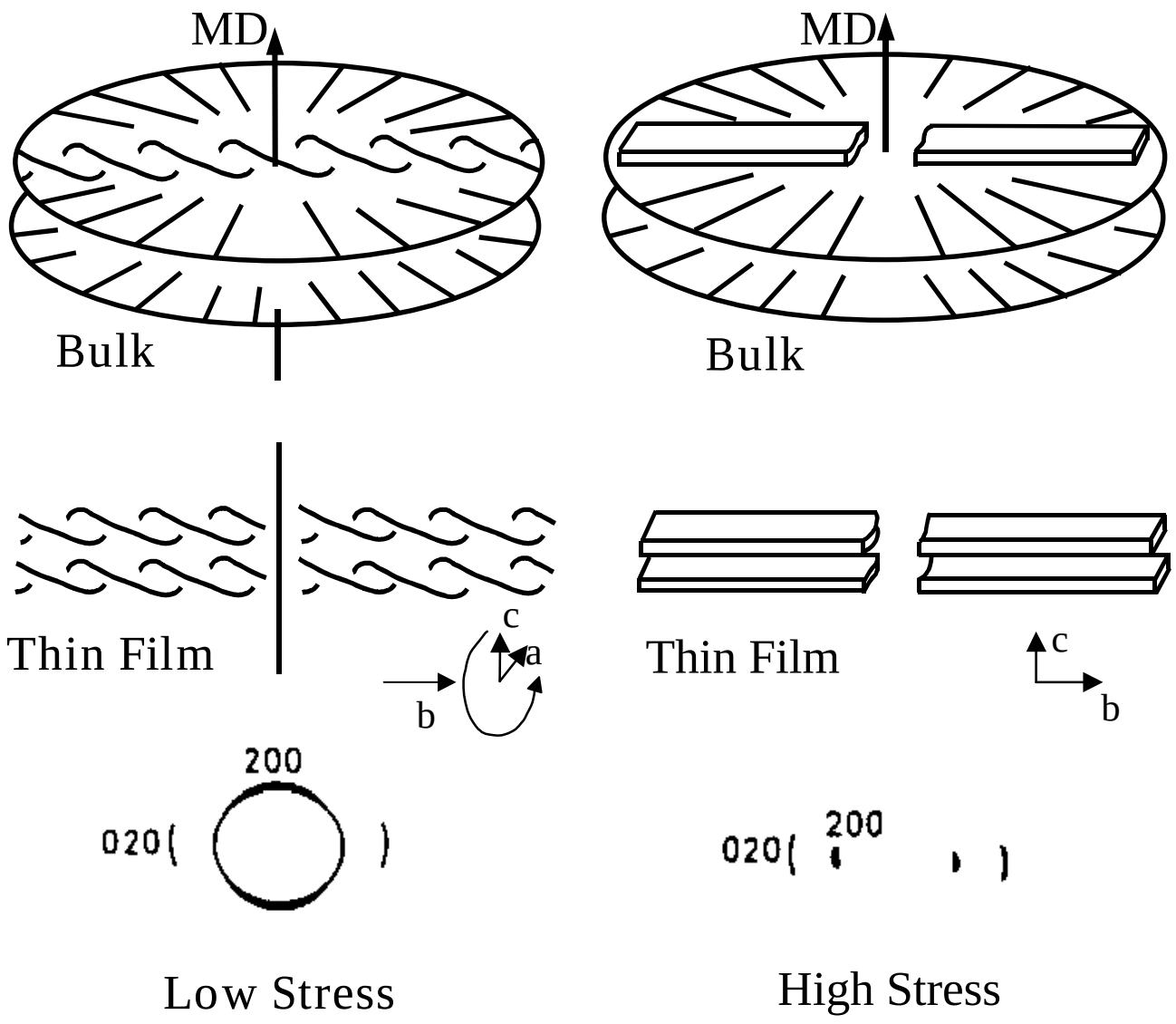

Figure 2.1[33] Schematic of the types of row structure with the respective extrusion condition and the main features of the PE WAXS patterns.

In the row-nucleated morphology, crystalline lamellae, composed of "folded" polymer chain(s), are formed perpendicular to the extrusion direction or MD. These stacked lamellar morphologies are formed in melt-extrusion processes when there is an orientational component of flow sufficient enough to produce preferential alignment of the chains in the flow direction. In contrast, quiescent crystallization occurs without the application of an orienting influence on the polymer chains. In this case, the spherulite is the common morphological structure observed. As an aside, the mechanical properties are very different between row-nucleated and spherulitic morphologies. Materials possessing row-nucleated morphologies possess mechanical anisotropy where spherulitic morphologies do not. In fact, some row-nucleated morphologies possess the ability to recover almost entirely after 100 percent extension perpendicular to the lamellae. Repeated deformation lowers the yield point but the degree of recovery remains basically constant.[1] Materials possessing these characteristics have been labeled "springy" or "hard-elastic".[34] The first hard-elastic materials were of iPP[35] and POM[36] and were discovered in 1965. An example of a tensile deformation curve for such a hard-elastic POM (Celcon) material, deformed along the MD, is displayed in Figure 2.2. For comparison purposes, Garber and Clark also included a non-elastic POM (Celcon) deformation response as observed in Figure 2.2. These authors were the first to show that the hard-elastic morphology is row-nucleated. Other polymers that can reportedly be produced into "hard-elastic" materials are, isotactic poly(1-butene)[37], polypivalolactone[38], poly(3-methylbutene)[39], and PMP[40].

As previously stated, annealing is utilized as the second stage in the MEAUS process for microporous film production. The importance of the annealing process for micropore formation was first observed by Sprague et al[2] and since by other investigators[4,41-44]. These investigators annealed a variety of semicrystalline films (e.g. PE, iPP, and POM) possessing stacked lamellar morphologies prior to their tensile deformation, specifically films characterized by a hard-elastic response. Annealing temperatures near the melting point of the polymer were

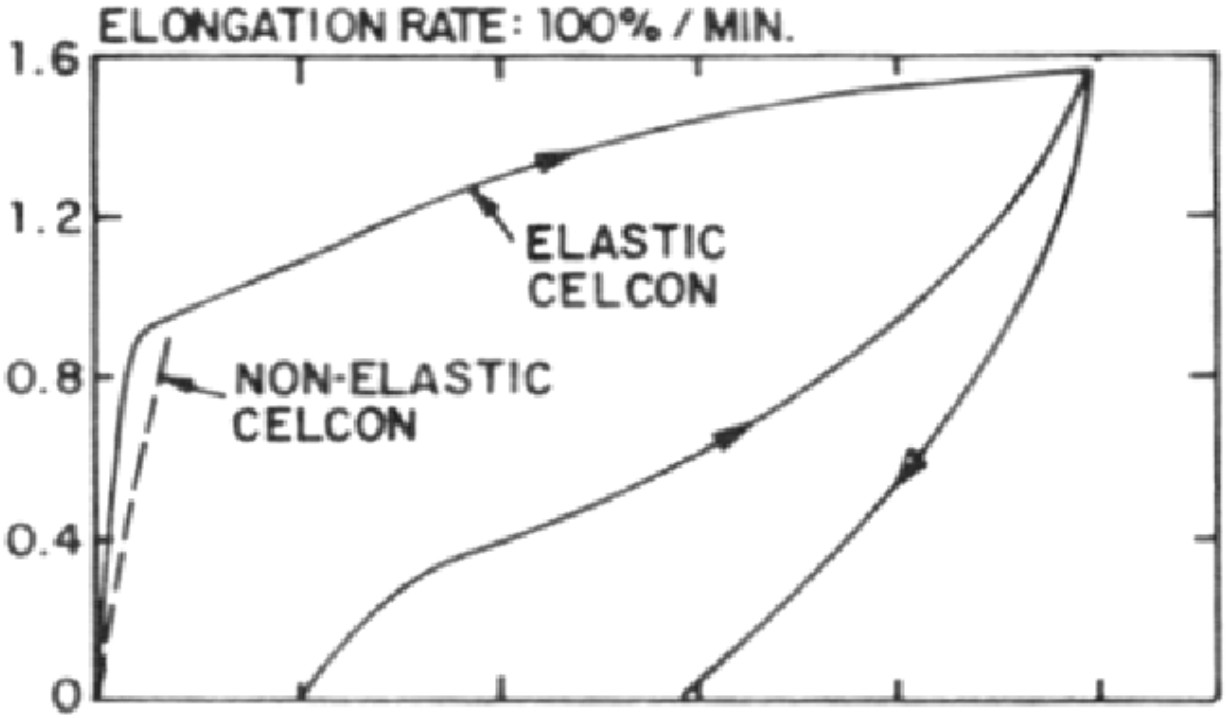

Figures 2.2 Tensile curves of hard elastic Celcon (POM) and non-hard elastic film obtained at –190°C.[36]

generally utilized in the study of Sprague et al. The response of the lamellae, as observed via small-angle X-ray scattering (SAXS), was an increase in the long spacing due to lamellar thickening. Lamellae thickening as well as lamellae perfection is a result of chain mobility via translational diffusion within the crystalline phase.[42] This diffusion process or relaxation is conventionally denoted as α_c. A variety of semicrystalline polymer types, for example PE and iPP, can display main chain mobility in the crystal phase and thus possess an α_c relaxation.

In the final MEAUS stage, the annealed films are subjected to a uniaxial deformation parallel to the MD followed by a thermal-relaxation/heat-setting step. The purpose of the relaxation step is to allow partial recovery of the film. A heat-setting step is employed after the relaxation so that the stretched film remains in approximately the same dimensions (i.e. recovery is kept at a minimum) after removal from the oven. Quynn and Brody studied the effect of uniaxial deformation on hard-elastic materials with SAXS, and noted that the interlamellar spacing increased in intensity and decreased in Bragg-angle (i.e. increasing d-spacing) upon deformation. The SAXS results were attributed to the formation of micropores, which increased in size upon greater levels of uniaxial deformation due to increased lamellar splaying/separation.[43] However, it was not until the work by Sprague et al that the nature of the microvoids was studied.[2,44] Their work discovered that a large number of interconnected microvoids are produced upon uniaxial deformation of the annealed film. In Figure 2.3, a scanning electron microscope (SEM) micrograph displays a microporous film where the micropores are evident throughout the cross-section of the film. It is noted that the microvoided morphologies produced via the MEAUS method are a consequence of interlamellar separation, which takes place at temperatures above the T_g of the specific *semicrystalline* polymer. This is in contrast to *amorphous* polymers which reportedly form voids, i.e. crazes or the process which is termed crazing, upon deformation at temperatures *below* their respective T_g.[45]

The MEAUS procedure briefly described above has been analyzed in the patent[5,38,46,47] and published literature[2,48]. Those corresponding authors have never attempted to set forth a list of criteria (i.e. prerequisites) that a semicrystalline polymer must possess to be considered viable for the production of polymeric microporous materials utilizing this process. *It is the principal goal of this study to propose a set of criteria, secondly to verify these criteria, and finally to investigate the results from resin to final film at each stage of the MEAUS process.* The reader may recall that the proposed criteria were previously listed in Chapter I. These criteria hold true for the semicrystalline polymers known to form microporous films via the MEAUS method, which includes PE and iPP. Both PMP and POM display chain relaxation in the crystalline phase (i.e. an α_c relaxation). In addition, these polymers possess relatively fast crystallization kinetics. Therefore, upon melt-extrusion of PMP or POM, planar stacked lamellar morphologies with "good" crystalline orientation should be feasible. In order to obtain these film characteristics (planar stacked lamellae and "good" crystal orientation), one should have an understanding of the individual uniaxial-stretching stages and the mechanisms that may potentially occur within each stage. To facilitate this understanding in terms of the melt-extrusion stage, some pertinent background information with regard to crystallization and the flow-behavior (melt and solution) of polymers will first be addressed.

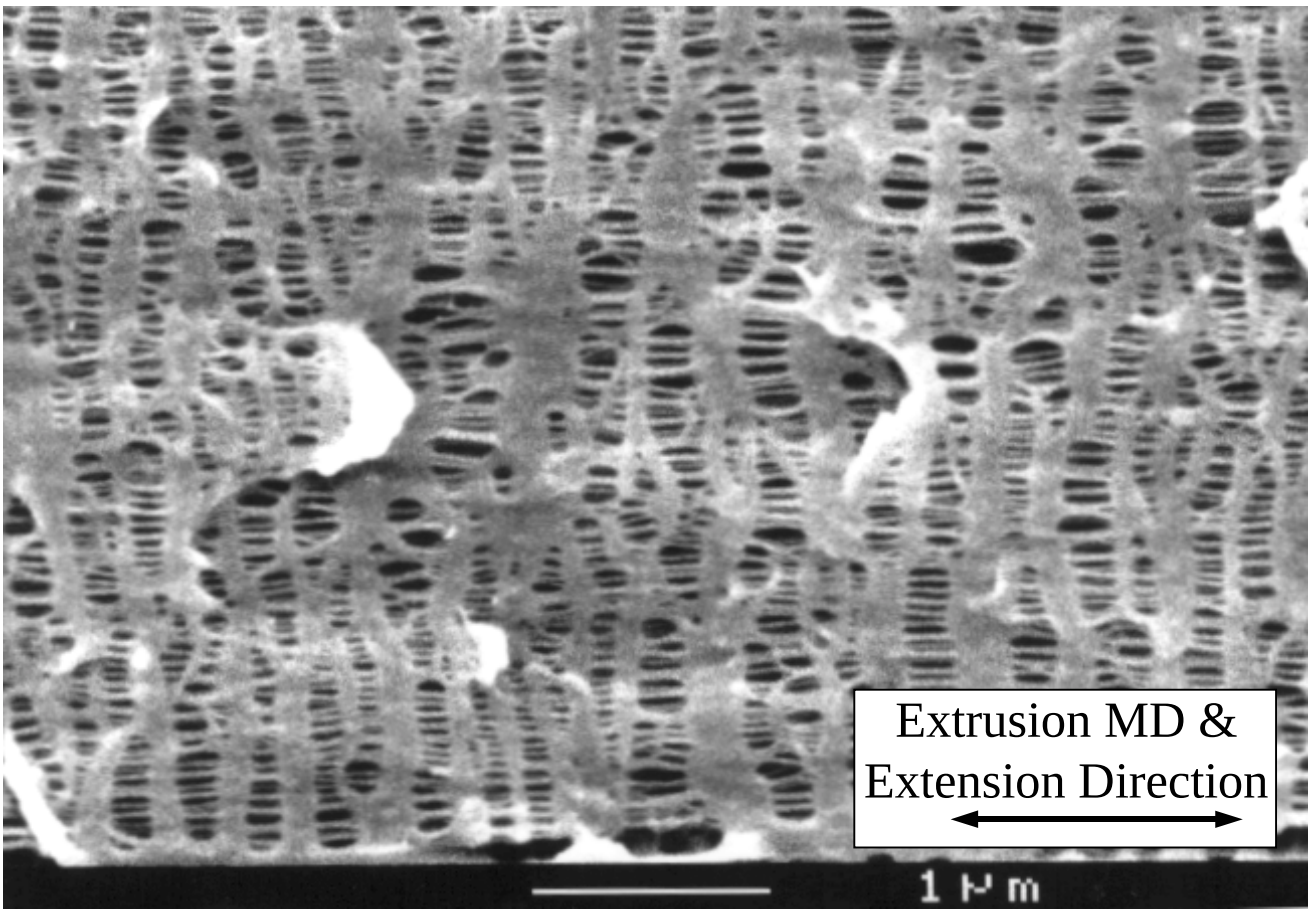

Figure 2.3 SEM micrograph of a microporous film cross-section displaying uniform microporosity throughout the film cross-section.

2.2 Crystallization Behavior with Emphasis on Flow Induced Morphologies

2.2-1 Crystallization:

A discussion of the general crystallization behavior of polymers and the resulting crystalline morphologies will be undertaken. One of the most common crystalline morphologies is the spherulite occurring under quiescent isothermal crystallization conditions. The spherulite is comprised of chain folded lamellae radiating outward from a central nucleation site with amorphous material existing between the lamellae. At a given supercooling ($\Delta T = T_m^o - T_c$), spherulites are known to grow at a constant radial rate ($\frac{dr}{dt} = \text{constant}$, where $r = \text{spherulite}$ radius) until spherulitic impingement where the crystal growth rate then terminates and secondary crystallization may follow.[52] In this case, supercooling is defined as the difference between the equilibrium melting point (T_m^o) and the isothermal crystallization temperature (T_c). Figure 2.4 illustrates a group of spherulites where impingement has occurred. Notice also the radial growth rings depicted within each spherulite. As the lamellae radiate from the spherulite center, the lamellae may often periodically twist, as is depicted in Figure 2.5, about the growth direction.

The linear crystal growth rate (G) has been divided into three regimes based upon the rates of substrate nucleation (i) and substrate completion (g). The crystal growth rate as influenced by the rates of substrate nucleation and substrate completion is depicted in Figure 2.6. Specifically in regime I, a crystal nuclei forms on the substrate followed by the remaining layer quickly filling with the same chain before further nucleation occurs ($i << g$). In Regime II, a large number of nuclei are formed before the substrate layer is completed ($i \sim g$). In regime III, catastrophic multiple nucleation occurs at a much greater rate than regime II ($i >> g$) thus essentially no substrate completion occurs.[49] These three regimes have been experimentally observed to depend upon the level of supercooling for a variety of polymers.

Figure 2.4 Schematic depicting spherulitic impingement and radial growth rings.[52]

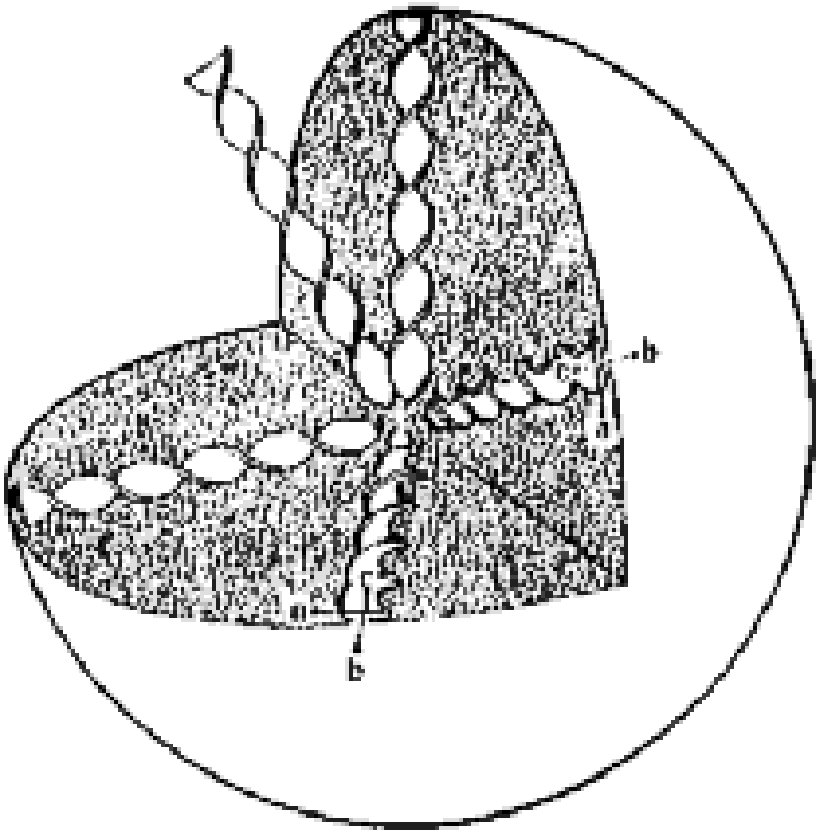

Figure 2.5[50] Schematic depicting a spherulite with twisting lamellae emanating from the spherulitic center.

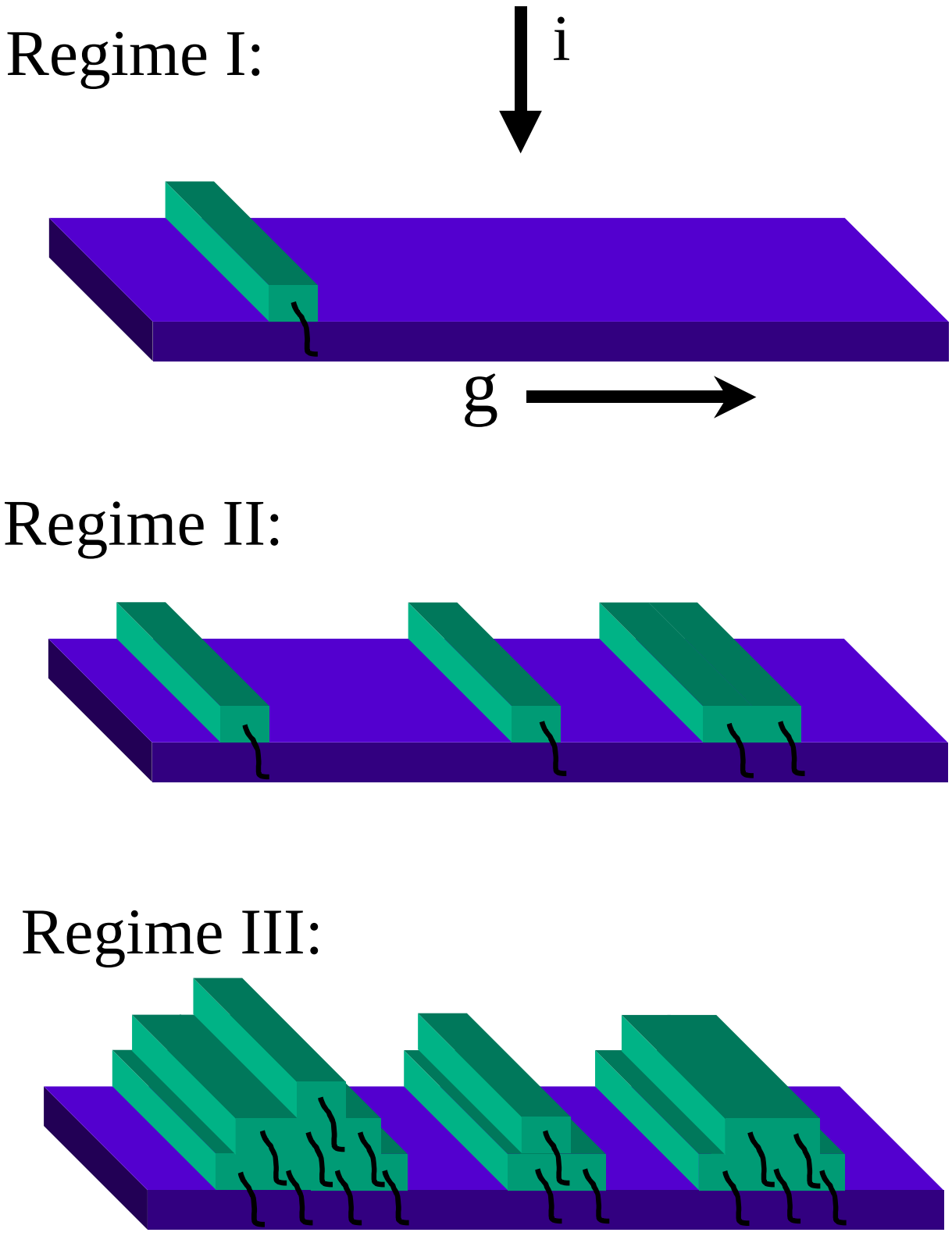

Figure 2.6 Schematic diagrams representing crystallization regimes I, II, and III where “i” is the stem nucleation rate and “g” is the substrate completion rate.

In order for crystal growth to occur, crystal nucleation must take place, which occurs by either homogeneous or heterogeneous means. Homogenous nucleation is a result of a single molecule or number of small molecules forming a nucleus of some size that is large enough to overcome the barrier for primary nucleation. The second and more common is heterogeneous nucleation in which nucleation typically occurs off a foreign particle. The foreign particle provides a surface to lower the free energy opposing primary nucleation, and as a result higher crystallization temperatures and greater nucleation rates occur.[52]

Heterogeneous nucleation, in some cases, takes place by a self-seeding mechanism and thus nucleation emanates from remnant polymer crystals, sometimes designated as the "melt-memory" effect.[51] As stated above, heterogeneous nucleation can also occur on foreign particles such as catalyst particles, dust, and designed nucleating agents. In the case of self-seeding, the number of nuclei has been found to be dependent upon the previous crystallization history (temperature and time), the time spent above the previous melting temperature, and the temperature at which this time was spent.[52] It was reported, for self-seeding nucleation, that the full elimination of memory effects (i.e. remnant crystals) at a fixed temperature scales to the 4^{th} power with weight average molecular weight (M_w) for isotactic poly-1-butene (PB-1) samples.[53] Self-seeding is also the nucleation mechanism by which row-nucleated lamellae occur where the nucleating sources are generally the extended-chain crystals that are a result of selected stretched chains in the melt. After the formation of these extended chain crystals, epitaxial overgrowth of the lamellae follows.[52] Strain induced crystals formed by drawing have also been found to provide nucleating sources for the epitaxial growth of lamellae.[54,55,52]

Prior to crystal nucleation, as proposed by Winter et al, there is a liquid-solid transition, he designated as gelation, which occurs very early in the crystallization process and initially is mostly composed of amorphous clusters.[56,57] As these clusters grow, overall molecular mobility begins to decrease. The critical gel point, defined by Winter et al as the onset of this liquid-solid

transition mentioned above, is where these growing clusters become impinged to form a loosely connected network low in crystallinity. At later stages of the liquid-solid transition, small-angle light scattering (SALS) patterns displayed two and four fold symmetry in the V_v and H_v modes, respectively. These patterns indicated the development of anisotropic morphologies. Light microscopy also showed closely packed but not fully developed spherulites suggesting crystallization had occurred albeit to a limited degree.[56]

2.2-2 Properties of Flow & Non-Quiescent Morphologies:

The crystalline morphology distinctly influences mechanical properties[58-60], and furthermore it is important in the formation of microporous films using the MEAUS process[4]. Thus, how a given morphology is obtained (i.e. the processing-structure-property relationship, PSP) is of interest.[12,61-63] From investigations of PSP relationships, a connection was proposed to exist between the level of chain extension in the melt (flow behavior) and the resulting crystalline structure (solid-state). Specifically, the degree of chain extension has been found to influence the final crystalline morphology, while the final morphology, as observed after crystallization, can serve as a window to the existing level of extension during melt-extrusion.[64] The pioneering melt-extrusion investigations by Keller and Machin[33] resulted in the proposal of two morphological models pertaining to the influence of the flow field as related to extrusion stress. These two models as they relate to extrusion stress are displayed in Figure 2.1, but will be discussed later in this section.

The influence of the flow field was first shown to be of significance in 1965 by the early work of Pennings and Kiel[65], whom found solution grown PE fibrous aggregates attached to a stirrer of a Couette apparatus operated at 50°C using dilute PE solutions. These fibrous aggregates were composed of a fine central thread consisting of extended chain crystals upon which nucleation and overgrowth of lamellae had occurred. These solution crystallized

structures were termed “shish-kebob” morphologies, schematically depicted in Figure 2.7. Because the shish-kebob morphology was first discovered in stirred solutions, where turbulent flow exists, it was difficult to characterize the cause of formation. Subsequent studies of these structures continued with a solution medium employing a wide range of polymers.[66-69] Pennings, van der Mark, and Booij in 1970[70] with the aid of a Couette apparatus concluded that the presence of “Taylor Vortices”[71] were critical for fibrous crystallization to occur because without Taylor Vortices fibrous crystallization was not observed. These authors further deduced that the longitudinal velocity gradient of the Taylor Vortices was the cause for chain extension.[72] Ziabicki[73], Peterlin[74], Pennings et al.[72] had previously mentioned the effect of the longitudinal velocity gradient on chain extension. Frank[75] was the initial investigator to describe this effect mathematically by first defining the velocity gradient as,

$$\dot{\varepsilon}_{ij} = \partial \boldsymbol{V}_j / \partial \boldsymbol{r}_i \qquad \text{(Eq 2.1)}$$

In Eq 2.1, **V** is the velocity at position **r**, and it forms a tensor that may be separated into symmetric ($a_{ij} = \frac{1}{2}[\dot{\varepsilon}_{ij} + \dot{\varepsilon}_{ji}]$) and anti-symmetric terms ($\omega_{ij} = \frac{1}{2}[\dot{\varepsilon}_{ij} - \dot{\varepsilon}_{ji}]$). Thus,

$$\dot{\varepsilon}_{ij} = a_{ij} + \omega_{ij} \qquad \text{(Eq 2.2)}$$

where the symmetric portion represents an extensional strain rate and the anti-symmetric portion represents a rotation rate. Longitudinal velocity gradients, an example being uniaxial extension, consist only of symmetric terms implying that ω_{ij} is equal to zero. This is the case for irrotational flow. In contrast, transverse velocity gradients possess a rotational rate that is not zero (i.e. $\omega_{ij} \neq 0$). Thus, the symmetric component (a_{ij}) is linked to the elongation of polymer chains in the direction of flow, and the rotational component detracts from the effectiveness of extensional flow.[59,75]

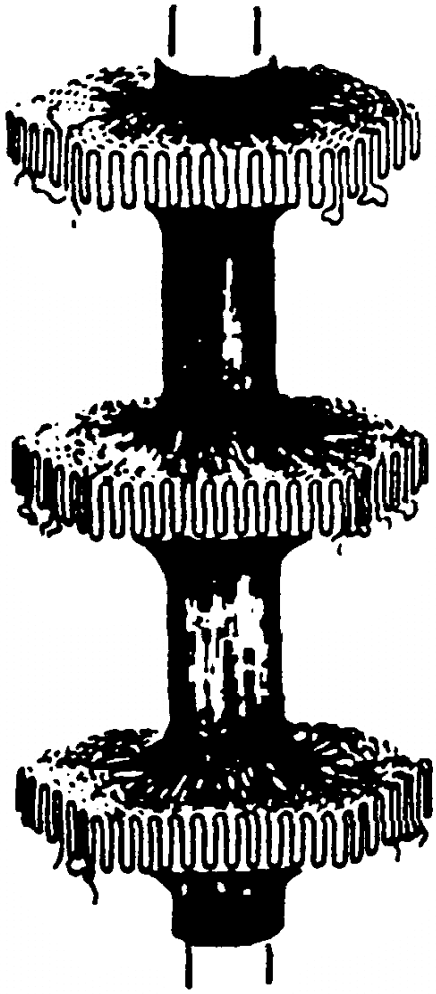

Figure 2.7[33] Schematic representation of the shish-kebab morphology.

From the studies involving polymer solution behavior, Keller et al.[33,76] first proposed the idea behind the row-nucleated model for nonisothermal crystallization of oriented melts. Specifically, the highly oriented extended-chain crystals act as nucleation sites for the stacked lamellar morphologies. These extended crystals are essentially thread-like structures stemming from the longer chain molecules which become stretched-out, or portions thereof, in the melt as a result of the application of the uniaxial orienting component of flow. In order to form extended chain crystals in flow, the longer polymer chain molecules must remain in an essentially stretched conformation during nonisothermal crystallization. Upon "quenching" a molten polymer capable of undergoing crystallization, a distribution of temperatures at which crystallization occurs will often be measured e.g. with dynamic scanning calorimetry (DSC). As a result, the crystallization temperature is nonisothermal, i.e., it was not held constant, and it is associated with the maximum in the measured crystallization exotherm. This definition of T_c and thus ΔT is in general used for flow processes and discussions of it, as is the case in this section. If no immediate quench is applied to the deformed melt, main chain polymer relaxation of the melt will occur. Fewer extended chain crystals results in a decrease in the nucleation density and thus a lower overall rate of nucleation. This phenomena has been demonstrated in numerous experimental works where orientation has been observed to enhance nucleation density and decrease gel time[56] as discussed in section 2.2-1. Orientational influences on nucleation are proposed to be a consequence of the entropy difference between the two melt states (i.e. $\Delta S = S_{oriented} - S_{unoriented}$), where the oriented entropy is lower than the unoriented (i.e. quiescent). Specifically, the nucleation rate in the high temperature range, $T > (T_m + T_g)/2$, has been defined by Yeh and Hong as[77]

$$\frac{N^o}{N} = \exp\left[\frac{\beta\sigma_e\sigma^2}{k_B T}\left(\frac{T_m^{o\,2}}{\Delta H_f{}^2 \Delta T^2} - \left(\frac{\Delta H_f \Delta T}{T_m^o} + T_m^o \Delta S\right)^{-2}\right)\right] \qquad \text{(Eq 2.3)}$$

where N^o is the nucleation rate in the oriented state, N is the nucleation rate in the quiescent state, k_B is the Boltzmann constant, ΔH_f is the heat of fusion. Since the first term in Eq 2.3 is greater than or equal to the second term on the right, faster nucleation under flow is expected. As an aside, entropy also play a crucial role in the melting temperature for both solution and melt processed semicrystalline polymers. Specifically, as entropy decreases, due to greater orientation in the melt, the melting temperature (T_m) increases. This can be explained thermodynamically by Eq 2.4 which occurs at the melting point of the polymer where under these conditions the free energy of the crystal equals the free energy of the melt ($\Delta G = 0$).

$$T_m = \frac{\Delta H_f}{\Delta S_f} \qquad \text{(Eq 2.4)}$$

In Eq. 2.4, the difference in entropy between the ordered crystalline phase and the melt is defined as ΔS_f, and the enthalpy difference between the crystalline phase and the melt is ΔH_f. The enthalpy change for an oriented melt relative to an unoriented melt will only be minimal where as the entropy change is not minimal and thus is often dominant in deciding T_m.[52]

As previously discussed, the maximum in the measured crystallization exotherm for a rapidly cooled molten polymer into its solid-state (i.e. nonisothermal crystallization) is often labeled T_c. This crystallization temperature is also affected by the amount of orientation within the melt. Specifically, higher values of T_c are a consequence of greater melt orientation. In the case of chain folded lamella, there is an inverse dependence of fold length (lamella thickness) on T_c or specifically supercooling (i.e. $\ell \propto 1/\Delta T$).[52,78] The crystallization temperature can also be influenced by the rate of cooling. Other factors being equal, faster quench rates will produce lower T_c values or larger supercooling, resulting in smaller lamellae thickness.

In addition to the possible influence of the extensional stress on lamellar thickness, it also has been observed to play an important role in the level of lamellar twisting. From the melt-extrusion investigations of Keller and Machin,[33] a lower stress condition, using PE, was found to produce row-nucleated morphologies possessing winding ribbon-like structures with the resulting diffraction pattern displaying both "c"-axis and "a"-axis orientation (Figure 2.1).[33] These authors further observed that a higher extrusion stress condition produced highly planar lamellar morphologies in which lamellae twisting was basically absent. The WAXS patterns of the higher stressed material displayed principally "c"-axis orientation. Keller et al further proposed that the extended chain crystals (thread-like precursors) are essential to the formation of a planar stacked lamellae morphology. According to Keller et al, the level of stress influences the concentration of the extended-chain fibrils which then influences the degree of lamellar twisting. Specifically, higher concentrations of extended-chain nuclei result from elevated levels of extrusion stress. Higher concentrations of extended-chain crystals then lead to greater numbers of nucleation sites and thus more numerous lamella impingement will occur. In other words, lamella impingement, i.e. the termination of primary lamella crystal growth by another lamella upon contact at the respective growing interfaces, is more likely to occur. The result is a decrease in the degree to which the lamellae can grow laterally and thus twist[64] as depicted in Figure 1.8. This theory was first proposed by Nagasawa[79] in 1973.

A more detailed explanation of Figure 2.8 will now be undertaken. As lateral lamellae growth occurs, which in the case of PE is along the "b"-axis, a gradual twist or oscillation/tilting around the direction of crystal growth takes place. Here the variable that determines the level of lamellar twisting or tilting and the overall crystalline orientation is the distance between nucleating fibers (i.e. the cylinder diameter in Fig 2.8). The cylinder diameter of Fig 2.8 is a function of the concentration of nucleating fibers in a given sample. Few fibers, or a small cylinder diameter in Fig 2.8, results in wide spacing between nucleating fibers in turn leading to

essentially spherulitic-like structures. In contrast, many closely spaced fibers, a large cylinder diameter in Fig 2.8, will produce partial to no lamellae twisting resulting in high chain orientation. This is a result of lamellar impingement occurring prior to significant twisting/tilting.[64,79] The problem with this theory, in some cases, is the lack of experimentally observable extended-chain fibrils even when a highly planar lamellar morphology exists.[4,33,80-82] In a specific study by Yu et al[4], two high density polyethylene (HDPE) resins differing in M_w but with similar M_n's, were melt-extruded at approximately the same condition. These two melt-extruded HDPE films possessed similar values of crystalline orientation, yet their morphologies were different. Specifically, the film produced from the higher M_w resin possessed evident extended-chain crystals whereas the lower M_w film did not, as studied utilizing TEM and WAXS. However, *both* films possessed planar lamellar morphologies with the lamellae of the higher M_w film being characterized by small lateral dimensions relative to the lower M_w film. In the case of the higher M_w film, the lateral lamellar dimensions and planar lamellar geometry were obviously affected by the extended-chain nuclei in the manner discussed above. Similarly, the lower M_w film possesses no evident extended-chain nuclei as a result the lateral lamellar dimensions are much greater, but its lamellae possess a planar geometry. According to Keller, the planar lamellar morphology of the low M_w film, or any film possessing a planar lamellar morphology without the presence of extended-chain crystals, may be accounted for by "micro-shishes" which are able to act as nucleating sites.[80] It was also suggested that the presence of tie-chains between lamellae could be possible remnants of these micro-shish structures.[81,82] In any event, the level of extensional stress applied to the melt strongly affects the concentration of nucleating fibers as well as the level of lamellar twisting. Specifically, stronger flow creates more extended chains in the melt. The resulting morphology generally possesses less lamellar twisting. In contrast, weaker extensional flow results in more lamellar twisting as well as fewer extended chains.

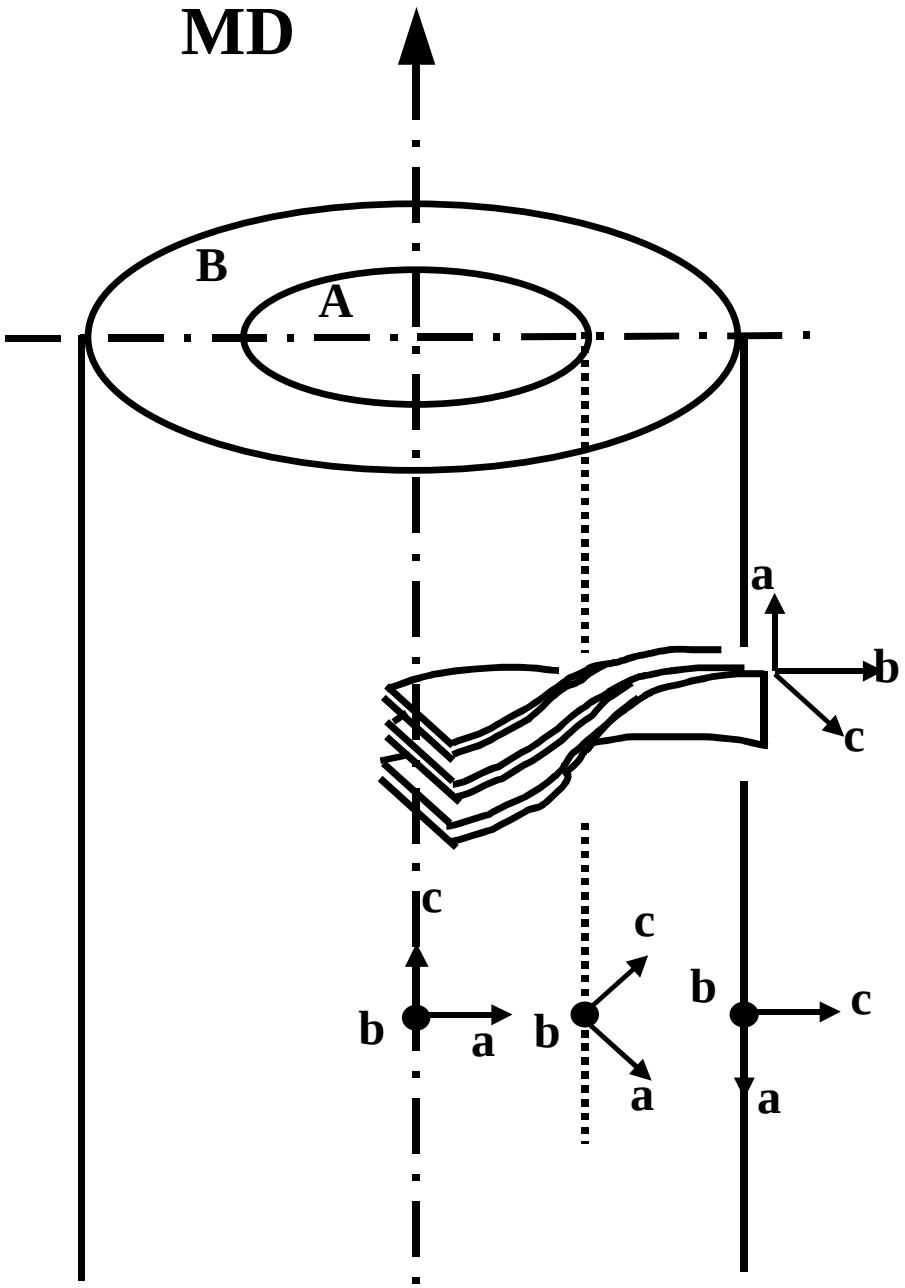

Figure 2.8[79] Scheme depicting the reasons behind intermediate orientations between predominant "c"-axis and "c"/"a"-axis orientation in terms of increasing diameter between row nucleating crystals as proposed by Nagasawa et al.

Keller et al attempted to further elucidate the relationship between the number of extended chains and the strength of extensional flow. To experimentally accomplish this, he utilized two opposing jets where a dilute solution of a given polymer was simultaneously drawn at a given strain rate into either orifice thereby creating a stagnation point directly between the two orifices. The orientation of the polymer solution was measured by observing the resulting transmitted intensity during flow between crossed polarizers.[64] From this, it was found that there are essentially two molecular stages of orientation in flow: the fully extended polymer chain (stretched) and the unoriented random coil conformation (coil). A lack of any intermediate conformations was also noted. The author writing this review has some concerns regarding the proposed lack of any intermediate conformations and other points of contention as will be addressed later. In any case, Keller et al observed that the strain rate at which a given molecular weight polymer goes through this conformational change (coil $\rightarrow$ stretch transition) is almost singular and thus termed the critical strain rate ($\dot{\varepsilon}_c$). As displayed in Figure 2.9, the transmitted intensity of the light is plotted as a function of strain rate for three different molecular weights. Prior to this work, the theoretical effect of elongational flow on an isolated random coil was calculated by de Gennes[83] resulting in the prediction of a sharp coil $\rightarrow$ stretch transition at a specific strain rate for a given molecular weight.

Figure 2.9 reveals a fact that is already common knowledge, for fixed conditions, longer chains are more readily extended given a specific rate of strain than shorter chains. It was also discovered that an upper strain limit exists for non-dilute solutions. Upon exceeding this strain limit, another type of critical phenomena pertaining to a critical strain for entangled networking ($\dot{\varepsilon}_n$) was said to exist. The relation between $\dot{\varepsilon}_c$ and $\dot{\varepsilon}_n$ was further found to be dependent upon polymer chain concentration as plotted in Figure 2.10. As this figure indicates, the higher the concentration, the lower $\dot{\varepsilon}_n$ becomes approaching $\dot{\varepsilon}_c$ where below $\dot{\varepsilon}_c$ the polymer chain conformations are random coils. For certain polymer concentrations and strain rates, there is a

zone above $\dot{\varepsilon}_n$ but below the formation of a completely networked system where extended and networked chains coexist. Between $\dot{\varepsilon}_c$ and $\dot{\varepsilon}_n$, however, the existence of a possible "window of extrusion" has been suggested[64,88] in which polymer chains can be extended without the formation of any network. In Figure 2.10, this "window of extrusion" includes solution concentrations equal to one, implying the ability to extend chains in the melt without the formation of a network. This further suggests that the entangled polymer chains are able to relax out of any long-lived chain couplings or so called "knots"[84]. Keller et al experimentally tested this theory by melt-processing narrow molecular weight distribution polymers (i.e. MWD ~ 1) using the opposed orifice apparatus. As previously done, the orientation of the chains as a function of strain rate was followed by measuring the intensity of transmitted through the system between crossed polarizers. Based upon this experimental setup, Keller et al suggested that the "window of extrusion" does exist.[64,88]

The processing window proposed by Keller et al[88] assumes that all chains go through a coil $\rightarrow$ stretch transition and thus are in a extended conformation. The ability for the chains to become extended is partly due to the nature of the apparatus used to test this prediction which allows some of the chains to remain subjected to the extensional stress indefinitely. Specifically, some of the chains may be caught at the stagnation point between the two orifices. This experimental apparatus is not necessarily practical for traditional melt-extrusion setups. In addition, resins possessing broad MWD's, will respond differently to a given set of extrusion conditions than a narrow MWD resin especially one that is nearly monodisperse. This difference is in large part due to the presence of a broader distribution of molecular weights which is thus characterized by different melt-relaxation times. Specifically, there are lower molecular weight chains which are characterized by faster relaxation times relative to their higher molecular weight counterparts.

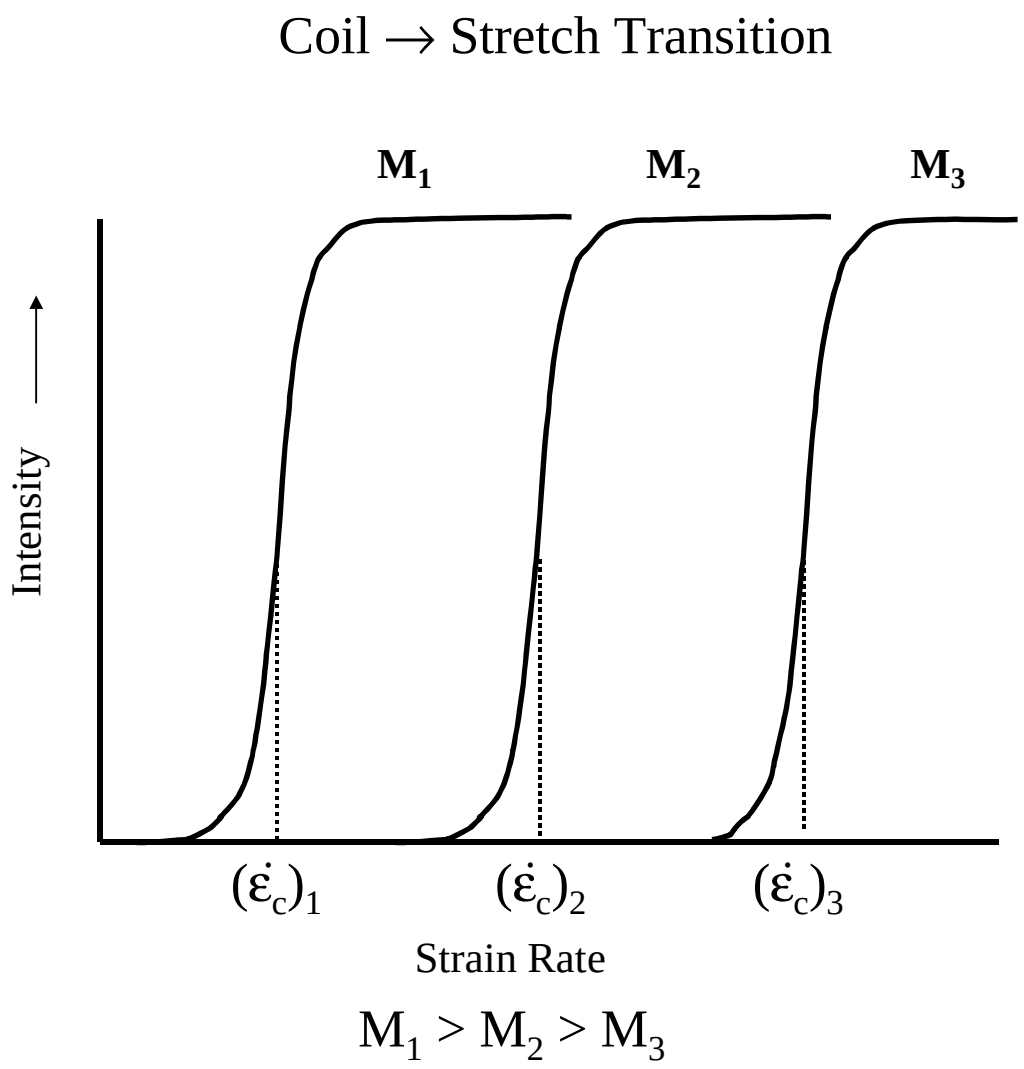

Figure 2.9 Plot of transmitted intensity of a dilute solution between crossed polarizers, i.e. birefringence, as a function of strain rate for three different molecular weights, where $M_1 > M_2 > M_3$, showing that the critical strain rate is dependent upon molecular weight.

Because of the faster relaxation times, these chains are not able to become extended due to insufficient strain rates. Thus, these chains remain in a more random coil conformation prior to crystallization. In addition, there is also the higher molecular weight species which are characterized by longer relaxation times during flow. According to the model of Edwards[85], these higher molecular weight chains possess longer "tubes" created by more numerous chain entanglements than the smaller chains. It is from these "tubes" or the entanglements defining them which the longer chains must reptate in order to become fully extended during flow.

Keller has suggested that if a resin is not processed in its "window of extrusion", an extended network of entangled chains will ensue at a sufficient strain rate. By adjusting the level of strain, the amount of extension the entangled network of chains experiences can be influenced.[86] Upon nonisothermal crystallization, the extended network is capable of producing row-nucleated morphologies where the type of morphology is controlled by the level of extrusion stress. For further information on this subject, reference 86 summarizes much of Keller's work in this area.

The type of mechanical degradation polymer chains experience has also been found to depend upon whether a independent polymer chain or an entangled networked of chains is studied. In the case of individual chains (e.g. in dilute solution), chain scission is found to occur after the molecule has been extended and is independent of other polymer chains (i.e. no entanglements). This type of degradation occurs as the strain rate increases along the plateau, displayed in Figure 1.9, to such an extent that the energy for bond dissociation is surpassed.[64] This critical strain rate is designated $\dot{\varepsilon}_f$, where $\dot{\varepsilon}_f > \dot{\varepsilon}_c$. In addition, independent chain scission has been observed to occur approximately in the center of the chain.[88] This type of mechanical scission is reportedly due to the symmetric nature of the flow field on the independent extended polymer chain because the location of maximum extensional stress is at the chain center. Only extended chains rupture indicating that the higher molecular polymer chains will undergo this

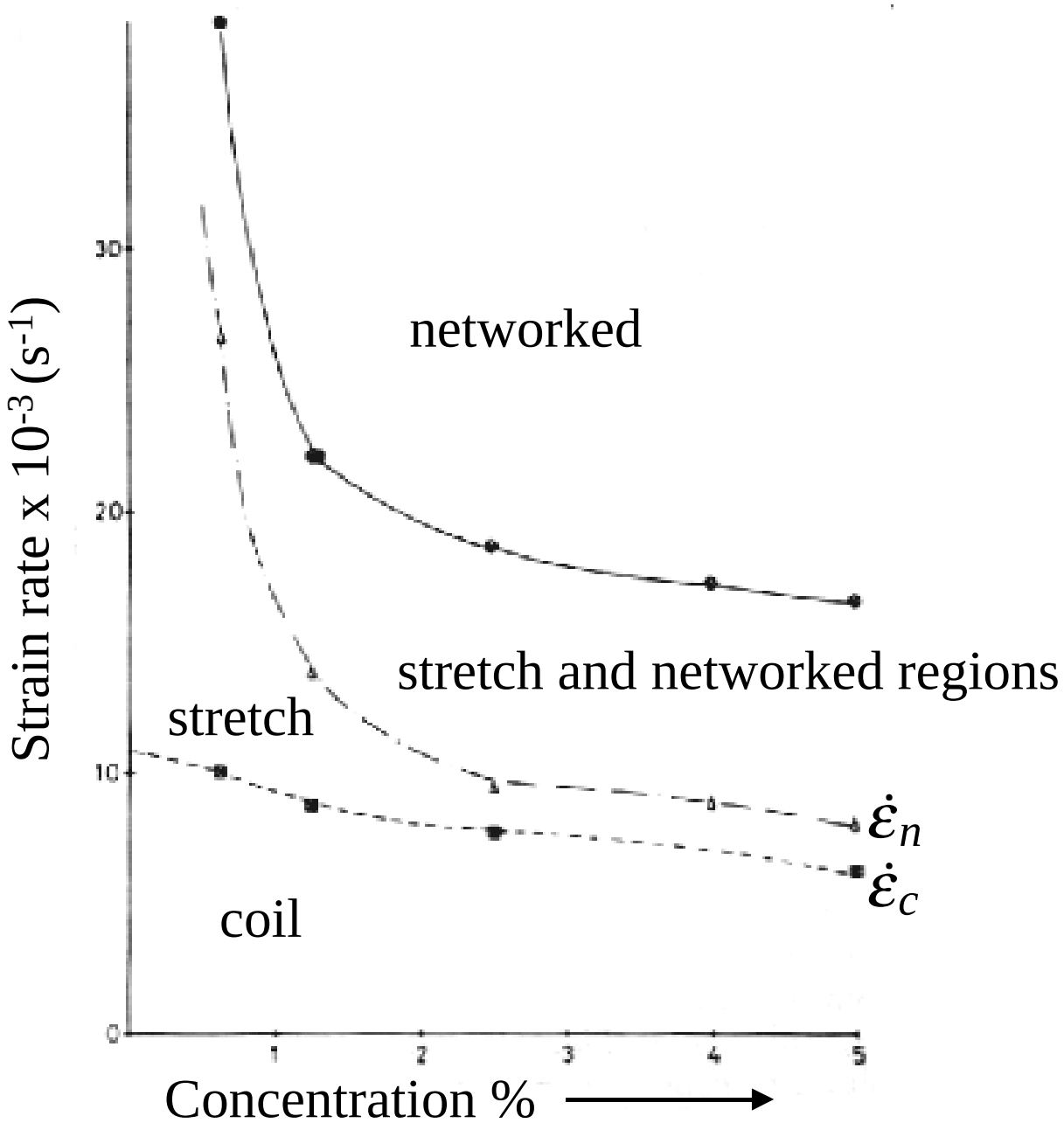

Figure 2.10 A Rate-Concentration-Transfer diagram of the development of connectivity as a function of concentration and strain rate, displaying ε_c and the critical strain to network formation ε_n for monodisperse ($M_w/M_n = 1$) a-PS in decalin soln. As reprinted from ref 62.

scission more readily than the lower molecular weight polymer chains.[88,87] As the polymer concentration increases, the randomness and frequency of polymer chain scission has been observed to increase. Thus, the location of the maximum stress changes along the chain backbone from the center of an independent chain to the points of entanglement for a transient network of entangled polymer chains.[88] It should be recognized that polymer chain degradation alters ε_c for given molecular weight and thus the extrusion window should be affected. Chain rupture or degradation pertains to the main chain covalent bond stability against any environmental (e.g. temperature) or mechanical factors. Basically two types of chain degradation occur in flow: mechanical (physically induced) as already discussed and thermal chain scission.[88]

In contrast to mechanical degradation, thermal degradation can for example occur because the ceiling temperature of the polymer molecule is approached.[88] The result is random chain scission throughout the length of the chain. This has an effect on the molecular weight distribution because "unzipping" of the chain occurs when the polymer ceiling temperature is approached. Thermal instability is especially important with regard to the C-O bond of POM.

2.2-3 Rheological Characterization:

From the above discussion of melt flow, predicting how a resin will respond upon melt extrusion (i.e. resin performance) is of obvious utility. Rheological characterization can often aid in furthering the understanding of a resin's processability. A common means of characterizing the melt-flow behavior of a resin is melt index (MI), however, this measurement represents the resin behavior at only a single temperature for a single deformation rate. Therefore additional rheological information a resin is required to obtain greater comprehension of the melt characteristics. Often small-strain oscillatory shear rheology provides a better overall description of the melt-flow behavior. The usefulness of this oscillatory shear data can be made greater if the data is fitted with a viscosity model. The Carreau-Yasuda (CY) equation is one such model. It

has found utility for a variety of polymer melts in part because each of its parameters can be correlated with physically meaningful melt-flow properties. The CY equation has the following form:

$$\frac{\eta(\dot{\gamma})-\eta_\infty}{\eta_o-\eta_\infty}=\left[1+(\tau_n\dot{\gamma})^a\right]^{(n-1)/a} \qquad \text{(Eq 2.5)}$$

where $\eta(\dot{\gamma})$ is the shear rate dependent viscosity, η_∞ is the infinite shear viscosity, η_o is the zero shear viscosity, τ_n is in general close to or slightly greater than the average of the melt relaxation spectrum.[89] The dimensionless parameter a describes the transition from Newtonian to shear thinning behavior (i.e. the "knee"). Specifically, it has been observed to be inversely related to the breadth of this zone. Hence a is an index of the relaxation spectrum breadth and has been found to decrease as MWD breadth increases according to Janzen et al.[89] The exponent (n-1) defines the slope of the $\eta(\dot{\gamma})$ versus $\dot{\gamma}$ curve within the power law region. Janzen et al have found that a value of n equal to 2/11 "adequately fits" the experimentally accessible viscosity data for most polyolefin melts they have analyzed, specifically linear polyolefins. For non-linear polyolefin resins, however, precisely low density polyethylene (LDPE), which is characterized by long chain branching, this value of n has been observed to produce inadequate approximations of the viscosity data.[90] The value of n equal to 2/11 was first proposed by Grassely in 1967[91] based upon a theoretical model of polymer chain disentanglement for narrow MWD systems.

If the empirical Cox-Merz rule, ($\eta(\dot{\gamma})=|\eta^*(\omega)|_{\omega=\dot{\gamma}}$)[92], is applied to Eq 2.5 the frequency dependent viscosity can be related to the shear-rate dependent viscosity. Further if the infinite shear viscosity (η_∞) is assumed to be negligible (a reasonable assumption according to Janzen et al since $\eta_\infty << \eta \leq \eta_o$) the simplified Carreau-Yasuda (CY) model, Eq. 2.6, can be easily utilized to fit complex viscosity data of a resin from oscillatory measurements.

$$\left|\eta^*(\omega)\right| = \frac{\eta_o}{\left[1+(\omega\tau)^a\right]^{\frac{(1-n)}{a}}} \qquad \text{(Eq 2.6)}$$

Where $\left|\eta^*\right|$ is the modulus of complex viscosity, ω is the oscillating frequency in radians per second which has replaced shear rate as the independent variable. From this discussion, a method has been addressed for analyzing the rheological properties by fitting the modified CY equation (Eq 2.6) to oscillatory shear data of a resin. From the CY parameters, one can have a better understanding of the processability of a given resin because of the physical significance each of the parameters. However, it should be kept in mind that these parameters are temperature dependent due to the temperature dependence of viscosity.

2.2-4 Tubular and or Blown Film Extrusion:

Tubular and or blown film extrusion has been used to control the resulting structure and orientation of semicrystalline polymers. Comprehension of how and why a given structure is formed has importance because of the effect it and crystal orientation have on the final film properties and uses. For this reason, what extrusion variables influence morphology[4,199] and the morphological types that can be produced[4,44,37] has received attention. Figure 2.11 is a schematic of a tubular blown film extruder. A description of the tubular film extruder and the associated process now follows. In the extruder, the polymer is melted where the melt is then pushed forward by the extruder screw through an annular die. As the melted polymer exits the die, an extensional component is applied to the melt via the nip rolls, which acts to draw the film upwards. Before the nip rolls are reached, air is introduced at the bottom of the die inflating the polymer tube. If the tube diameter is greater than the die diameter, a stress along the hoop direction or transverse direction (TD) occurs and thus a biaxial oriented film results (i.e. tubular blown film). The ratio of the tube diameter to the die diameter is termed the blowup ratio (BR);

thus, in the above case BR is greater than one. If the extruded tube diameter is equal to the die diameter (i.e. tubular film extrusion) the BR is equal to one, and the orientation is only uniaxial along MD.[4] After exiting the die, the polymer is quenched and solidified at or above the air ring for a given flow rate. The resultant film morphology has largely been determined to be a function of the temperature of extrusion, stress applied during extrusion, quench dependent parameters (quench height, air ring gap, airflow rate), and polymer resin characteristics (molecular weight, chain architecture, comonomer, etc.).

A useful dimensionless number when discussing processing conditions in relation to characteristic polymer relaxation times is the Deborah Number (D_e) defined as

$$D_e = \frac{\text{Molecular Response or Relaxation Time}}{\text{Experimental or Observation Time}} \qquad \text{(Eq 2.7)}$$

Specifically, if the Deborah number is greater than unity the molecular response time is longer than the experimental time, and the material behavior is solid-like (elastic). If the Deborah number is less than unity, the molecular response is more liquid-like (viscous). That is the response time of the polymer molecules is short relative to a given experimental time. For example, a higher extrusion temperature influences the Deborah number by decreasing the relaxation time for a given experimental time window. As a result, the Deborah number would decrease thereby suggesting more of a liquid-like response. This melt response equates to fewer extended chains implying a relative decrease in the number of fibril nuclei upon crystallization. Similarly, the experimental time frame can be affected by changes in the rate at which extrusion occurred, e.g. extrusion rate and line speed. Specifically, if the line speed is decreased, the experimental time is increased while the melt-relaxation time will remain essentially constant. Thus, the Deborah number will decrease suggesting again more of a liquid-like response.

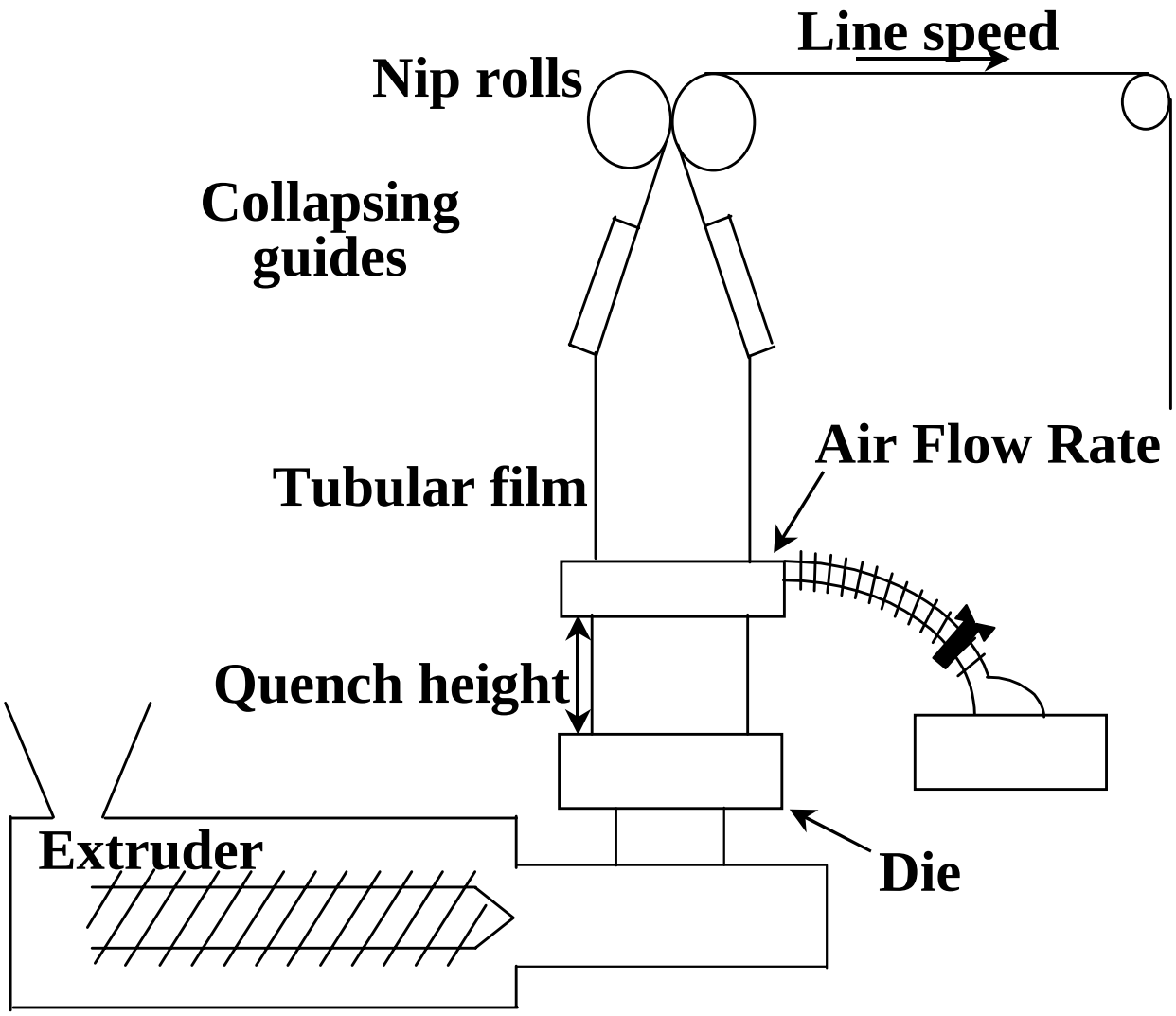

Figure 2.11 Schematic of tubular film process and key components.

There have been a wide range of studies investigating tubular (BR=1) or blown (BR>1) film extrusion and the effect melt-extrusion conditions on film properties. Techniques such as SAXS[4,37,93-96], wide-angle X-ray scattering (WAXS)[4,37,97,98] or X-ray pole figure analysis[93,94,96-100], birefringence[4,97,99,104,101], electron microscopy[4,95,104], infrared dichroism[4,102], atomic force microscopy (AFM)[95], and light scattering[37,103-105] have been utilized to follow the influence of the processing conditions. While many of these investigations pertain to PE[4,33,100], others have utilized iPP[106-108], PB-1[37,101], and isotactic polystyrene (iPS)[101]. From these investigations with the exception of iPS, the resultant morphology is generally composed of lamellar rows, which are for the most part perpendicular to MD. As stated earlier, these lamellae nucleate from a central core of extended chain crystals (thread-like precursors). The number of these extended-chain crystals increases with increasing strength of flow during melt-extrusion resulting in less lamellar twisting.[64]

Light scattering has in some instances been employed to observe structures on the order of the wavelength of light (4000-7000 Å). For example, H_v SALS (horizontal polarizer and vertical analyzer) of undeformed spherulitic configurations typically yields a symmetric four lobed pattern termed cloverleaf which possesses four-fold symmetry.[109] As previously discussed in section 2.2, such spherulitic-like superstructures are not normal for flow induced morphologies. In the case of PE shish-kebobs obtained from stirred solution, the SALS patterns, Figure 2.12, display 2 fold symmetry and are not cloverleaf-like.[110] In the same study, light scattering was employed for analysis of a tubular extruded iPP film possessing stacked lamellae where the typical H_v cloverleaf pattern was also not observed, see Figure 2.12. For PB-1 tubular extruded films, studied by Hashimoto et al.[37], butterfly-type H_V SALS patterns occurred. These SALS patterns were interpreted as stemming from isolated “fans” (sheaf-like structures) composed of two identical opposing sectors oriented preferentially normal to the MD. The authors indicated that fibril structures oriented along the MD are the nuclei for these sheaf-like morphologies. A

surface replication along with the corresponding H_V pattern of these structures and the proposed model are displayed in Figure 2.13.

The above discussion summarizes many previous works. It also hopefully helps convey to the reader an understanding of flow-behavior, methodologies for resin melt-flow characterization, and possible crystalline morphologies. These subjects have been addressed because of their importance to the MEAUS process for microporous film production and more specifically to the first stage, which is tubular melt-extrusion.

a)

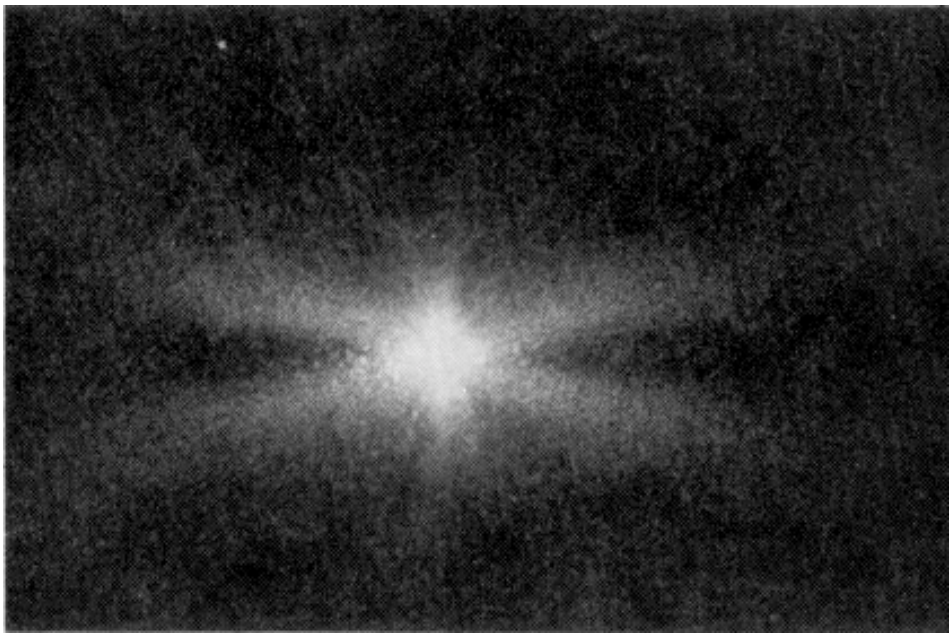

b)

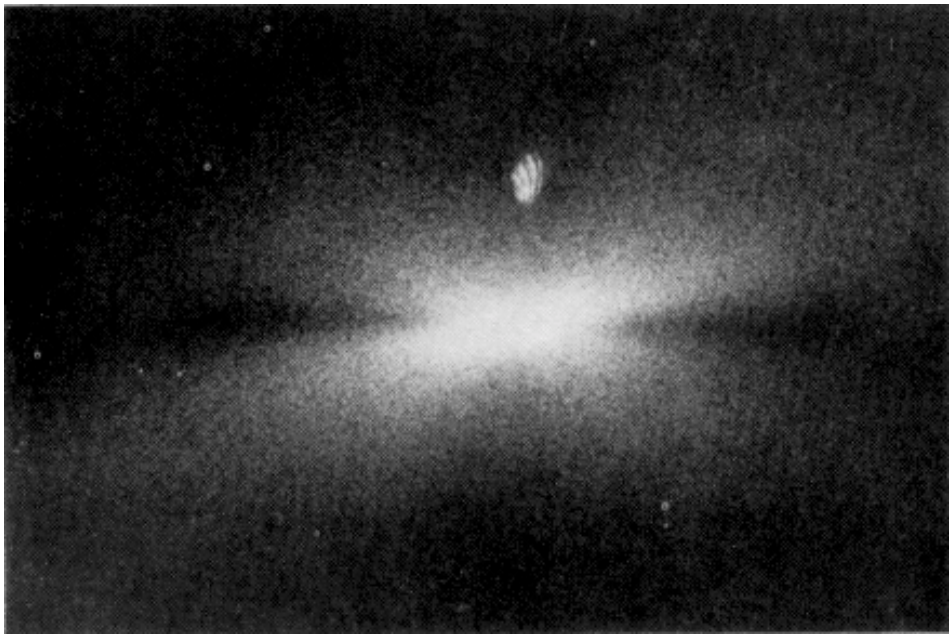

Figure 2.12 H_v SALS patterns of a) tubular extruded iPP film and b) stirred solution grown shish-kebob morphologies.[110]

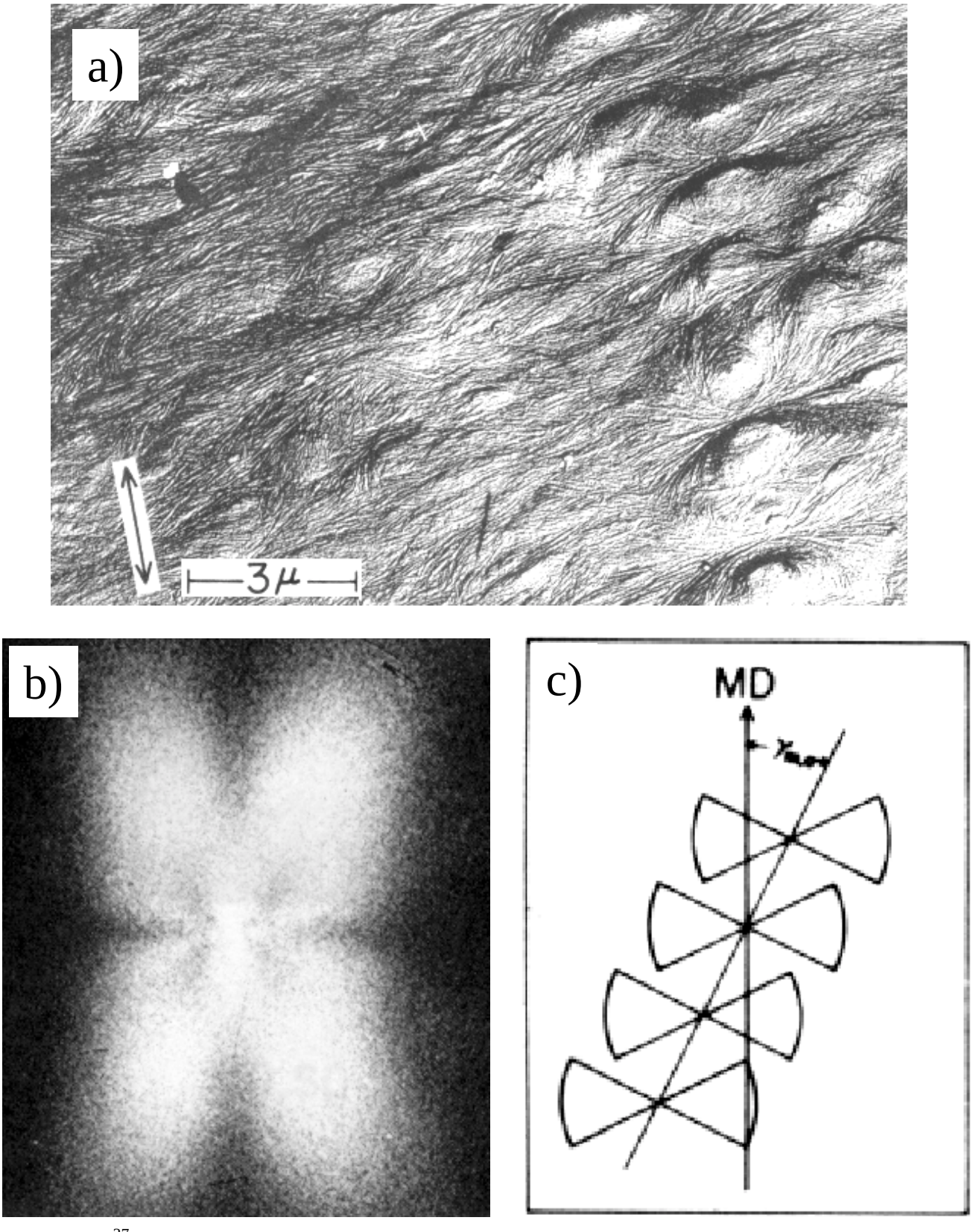

Figure 2.13[37] PB-1 tubular films a) surface replication of the sheaf-like structures, b) SALS H_v pattern of the PB-1 film, and c) proposed model accounting for these structures.[37]

2.3 Thermal Annealing & the Crystalline α_c Relaxation

2.3-1 Thermal Annealing of Semicrystalline Polymers:

After melt-extrusion, the second step in the MEAUS process is annealing of the film to induce perfection and thickening of the crystalline lamellae. The effect of annealing conditions on polymer orientation, morphology, and crystallinity has received attention.[4,52,111] The annealing effect has also been studied by following molecular mobility in addition to physical and mechanical property changes. Yeh et al has proposed several variables deemed critical to understanding annealing.[111] These variables are temperature, time, heating rate, prior physical state (e.g. drawn vs. undrawn or single crystal vs. bulk), thermal history, chemical architecture, and polymer resin composition (molecular weight, degree of branching, etc.).[111]

In summary of past annealing investigations, two principal models have been proposed that describe the resulting morphological and crystalline mobility (α_c relaxation) changes. Generally, it has been accepted that these two models can be applied separately or simultaneously depending upon the annealing conditions. The first model applies to fast heating rates and annealing temperature(s) close to the melting point whereby the thinner lamellae first melt and then recrystallize into thicker lamellae. The conditions of the second model include slower heating rates with the annealing temperature(s) closer to the temperature of crystallization resulting in thicker lamellae by a diffusion mechanism (i.e. α_c relaxation).[112] The α_c relaxation is associated with main chain translational mobility of nonchemical defects along the polymer chain backbone in the crystalline lattice upon annealing at sufficient temperatures.[113,114] This mobility within the crystalline lattice also allows for greater crystalline perfection. Crystal thickening indicates that the polymers are thermodynamically metastable, and the thickening process can be considered as going from a higher energy state to one of a lower energy state. The thermodynamic metastability of the crystalline phase is a consequence of the crystallization kinetics that can

control lamellae thickness, as previously discussed. Because of the crystalline mobility (α_c relaxation), the amorphous region conformations can also relax to less constrained states.

2.3-2 The Crystalline α Relaxation (α_c) :

Many polyolefins, halogen substituted polyolefins, and polyethers possess an α_c relaxation. Specific polymers that have been shown to possess an α_c relaxation are polyethylene[115], isotactic polypropylene[116], PMP[117], polytetrafluoroethylene[118], poly(vinylidene fluoride)[115], poly(ethylene oxide)[115], and polyoxymethylene[115]. Rault suggests that other polymers experience a mechanical α_c relaxation, e.g. poly(ethylene terephthalate), nylon6,6, isotactic polystyrene, and poly(etheretherketone). However, the thermal energy required for activation is high enough to be convoluted with crystal melting.[119] This higher energy relaxation is due to greater chain rigidity or secondary bonding present in these systems.

Crystalline mobility or reorientation of the chains within the crystalline phase has been identified by Boyd and Mansfield as a twisting or screw dislocation of the polymer chain through the crystal lattice causing main chain diffusion.[113,114,120] In the case of PE, the mechanism was defined as a "smooth" twisting of the C-C skeleton. The Mansfield-Boyd theory depends upon initial crystalline layer thickness. According to their theory, an α_c relaxation distribution results because a distribution of lamellae thicknesses exists. The peak of the α_c mechanical relaxation distribution is termed $T_{\alpha c}$.

McCrum, Read and Williams[121] and Hedvig[122] have discussed the data and opinions of various researchers regarding α_c relaxation whether it is observed via mechanical spectroscopy (DMA), dielectric, or solid state nuclear magnetic resonance (NMR). There is general agreement that the source of the α_c relaxation, when observed by solid state NMR or dielectric testing, is the crystalline phase.[114] The exact source of the mechanical α_c relaxation has been of considerable debate.[42,113-122,127-129] It was determined that the dielectric (or NMR) α_c relaxation times are

much faster than those of the mechanical α_c relaxation, as observed in Figure 2.14 for PE samples at 50°C, with the relaxation times for all processes depending upon lamellar thickness.[123] In addition, the mechanical α_c relaxation is dependent upon different levels of crystallinity. Specifically, the magnitude of the α_c relaxation has been observed to decrease with increasing amounts of crystallinity yet is never completely eliminated at 100 percent crystallinity as has been calculated theoretically.[114] Thus, Boyd has suggested that the crystalline chains can initiate the molecular motions which then propagate into the amorphous phase where the mechanical relaxation is the measured response of main chain crystal translation to the constrained amorphous regions.[113,114]

The effect of tension/deformation on the α_c relaxation has also been examined, specifically with regard to PE[124] and polyvinyl alcohol (PVA)[125]. For PE, Ward et al observed that the mechanical α_c relaxation shifted to slightly lower temperatures and decreased in magnitude with increasing amounts of uniaxial deformation (i.e. increasing crystal orientation). The mechanical α_c relaxation of PVA similarly decreased in magnitude with increasing draw or increasing crystal orientation, but unlike PE, the PVA relaxation shifted to higher temperatures with draw. As indicated by the author with respect to PVA, neither the effect of increasing orientation, increasing crystallinity, or prior morphology can solely be used to explain the response of the mechanical α_c relaxation for PVA.[125] No comment was made, however, with regard to the cause-effect relationship of tension on the PE α_c relaxation. In addition to the effects of tension on the α_c relaxation, Yeh et al. determined that tension was a significant variable in observing the general annealing behavior of polymers.

Chain symmetry was another of the annealing variables mentioned by Yeh et al.[111], and it has also been observed to be of consequence pertaining to the α_c relaxation[114,119]. As stated above with regard to the α_c mechanism described by Boyd, the essential feature is the ability to form a

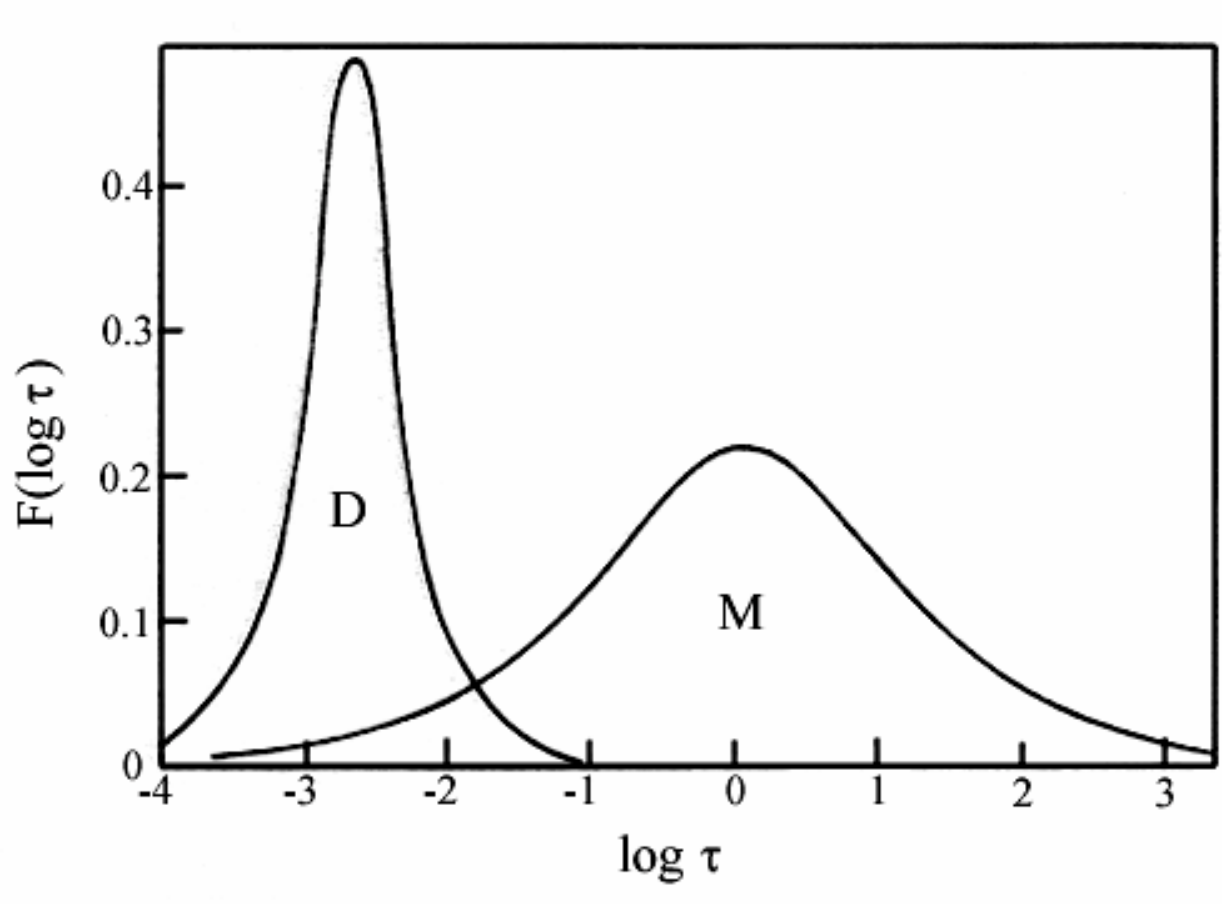

Figure 2.14 Dielectric (D) and mechanical (M) α_c relaxation distribution times for similar PE specimens at 50°C.

mobile entity within the crystal that can advance translationally. If chain symmetry is lacking, the energy barrier for chain translation is much higher than if symmetry exists. This is because the chain needs to remain in crystallographic register with its neighboring chains once the defect has migrated past its previous position.[42] This higher energy barrier to activation explains why some semicrystalline polymers lack an α_c relaxation because they possess large bulky groups or repeat units which are not highly symmetric.[114,119] Chain imperfection should have the same effect. Therefore, when a homopolymer does possess an α_c relaxation, the addition of comonomer and/or branching should have an effect upon crystalline mobility by disrupting the chain symmetry. Specifically, Yasuda et al. found for PE that the activation energy increases linearly with increasing methyl branch content. It was concluded that with addition of comonomer, crystalline mobility was hindered resulting in less chain to chain slippage.[126]

It has also been recognized that ultradrawing and solid-state processing of polymers possessing the α_c relaxation is possible, and polymers not possessing the α_c relaxation are not able to undergo either ultradrawing or solid-state processing.[61,125,127-129] Thus, the α_c relaxation appears to facilitate these two processes. Ultradrawing is defined as achieving draw ratios (L/L_o) greater than 20 where L is the final sample length and L_o is the initial sample length. In ultradrawing, the chains are not pulled straight through the crystal, but they proceed through the crystal via thermally activated helical jumps (i.e. α_c relaxation).[63,113,134] The results suggested that the applied stress, temperature, and rate of drawing are of importance to ultradrawing which is in accord with many of those annealing variables proposed by Yeh. et al.[111]

For PMP, there has been only limited studies of its annealing behavior. Further, according to Rault, since PMP possesses a large side group which should increase steric hindrance and result in greater chain rigidity, the PMP α_c relaxation should not be large in magnitude or breadth. This relaxation should also reside close to the crystalline melting peak.[119] As will be shown in the

next section, however, the PMP mechanical α_c relaxation is relatively large in magnitude with the relaxation breadth encompassing the entire temperature range between its T_g and T_m.

2.3-3 PMP α_c Crystalline Relaxation:

Poly(4-methyl-1-pentene) has been observed to possess both a crystal (α_c) and lower temperature T_g relaxation (β), as displayed in Figure 2.15. This relaxation has been studied by DMA and solid state NMR analysis.[130,131] As Figure 2.15 shows, under the test conditions and thermal history of these samples, the onset of the α_c relaxation for either material occurs at approximately 50°C reaching a maximum (i.e. $T_{\alpha c}$), depending upon cooling history, of 100 to 150°C and continues up until melting of the crystalline phase around 240°C.[132] It is generally accepted that translation of the 7/2 helix, or any crystalline helical conformation, through the crystalline register occurs via “helical jumps”, as has been observed with NMR.[133,134]

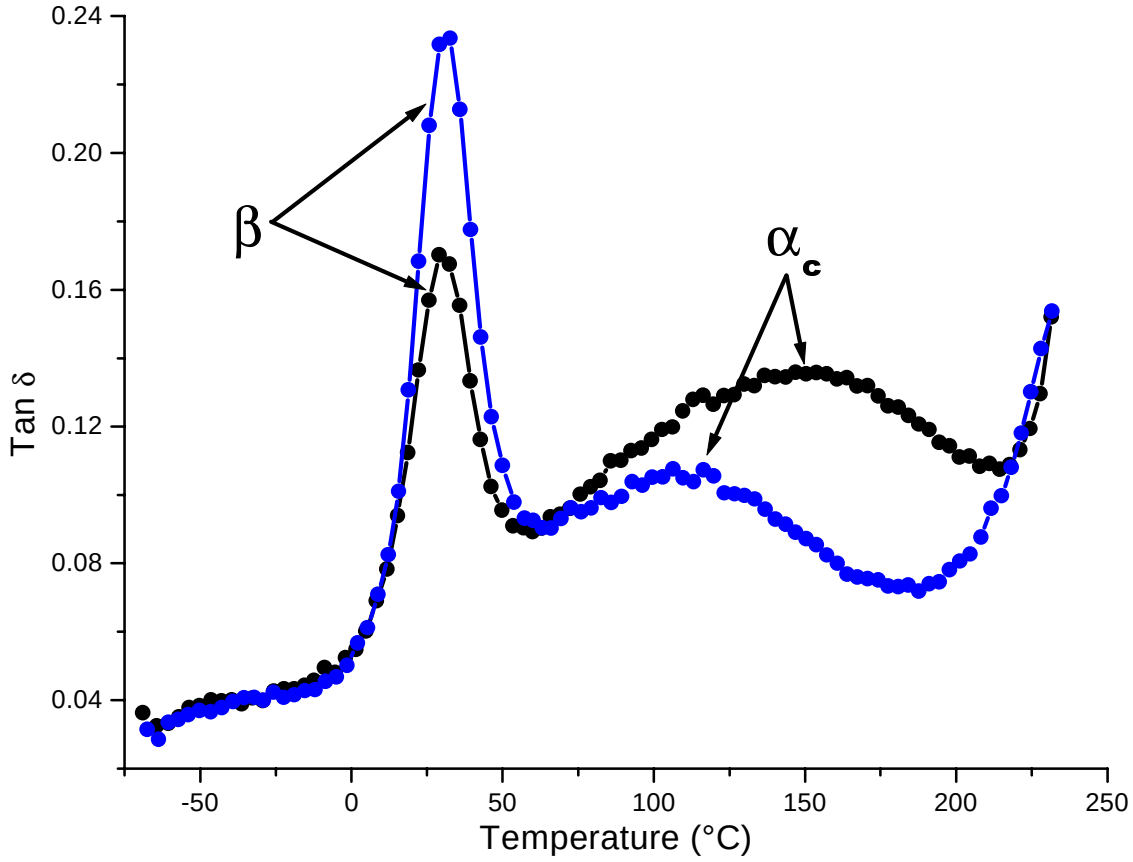

Figure 2.15 DMA Tanδ response of a PMP (-●-) slow cooled and (-●-) quenched compression molded samples as a function of temperature using a heating rate of 2°C/min at 1Hz.

2.3-4 POM Relaxations:

Like PMP, POM also crystallizes into a helical conformation (9/5 helix) and possesses the ability for crystalline mobility (α_c relaxation).[42] The other relaxations of POM, however, have been of some controversy even though extensive study via DMA, dielectric, and solid state NMR has been accomplished. Thurn[137], Read & Williams[138], Arisawa et al.[142], Williams[135], and Ishida et al[136] have studied the POM dielectric response. In addition, the mechanical relaxations have been studied by Thurn[137], Read & Williams[138], McCrum[139], Takayanagia[140], Eby[141], Arisawa et al[142], Wetton & Allen[143], Bohn[144], and Keating et al[145]. Figure 2.16 illustrates the mechanical spectra for two POM samples differing in rate of cooling. Clearly, three distinct relaxation peaks are evident and are designated in order of decreasing temperature or α (110-125 °C), β (-10 °C), and γ (-75 °C).[119-131] The main relaxations of interest for POM have been the γ & β transitions where both have separately been attributed to the onset of cooperative segmental motion.[121] These two relaxations have been shown to occur within the amorphous phase and must originate from the main chain due to the absence of branches in POM.[146]

Knowledge of the glass transition temperature is of importance in the MEAUS process. Specifically, the stretching stage requires knowledge of T_g because the deformation occurs at temperatures that must be above T_g as explained below in Section 2.4. Past investigations attempting to elucidate which relaxation (β or γ) is attributed to the glass transition of POM are now described.

Some of the first work on POM relaxations was done by Read and Williams, who observed from dielectric and mechanical results only the α and γ relaxations.[138] They suggested that the γ relaxation is the glass transition based on the large peak size. Later, McCrum, Read, and Williams suggested the β transition to be the glass transition.[146] Kazen and Geil utilizing POM films provided direct morphological evidence upon uniaxial deformation of the films at room temperature. These researchers concluded that the glass transition is in *not* at –70°C,

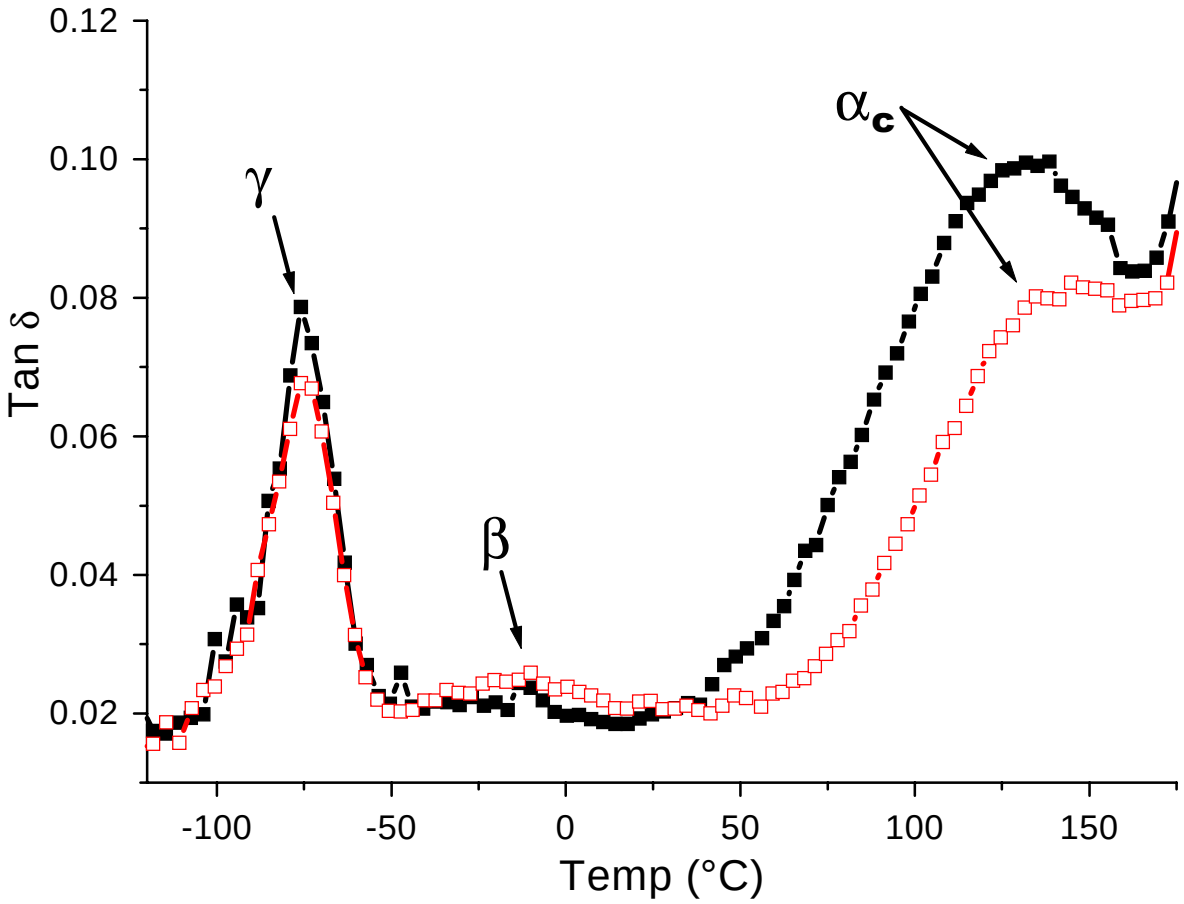

Figure 2.16 Tanδ response of Delrin 100 POM (-■-) slow cooled and (-□-) quenched compression molded samples as a function of temperature using a heating rate of 2°C/min at 1Hz.

corresponding to the γ process, but that the glass transition *is* the β process.[147] In addition, Bohn discovered that upon copolymerization of poly(ethylene oxide) (PEO) with POM, the β peak *is* enhanced by the resulting decrease in crystallinity and thus concluded it to be the glass transition. Another method to elucidate the POM glass transition was to use a miscible blend of POM and a oligomer or other polymer. The resulting effect on the mechanical response with increasing blend component fraction was then analyzed.[145] The investigators observed a shift in the mechanical β peak while the mechanical α and γ peaks remained unchanged.[145] As a result these investigators attributed the β relaxation to T_g. Finally, McCrum studied the dependence of the POM mechanical response with respect to thermal history and effect of H_2O on POM. Upon aging a freshly cooled specimen for "several weeks" at room temperature, the β peak magnitude decreased significantly versus a freshly cooled sample. No effect of thermal history on the γ relaxation was observed. In addition, small levels of absorbed water was found to increase both the β and γ transition magnitudes versus dry POM samples indicating a kind of plasticization effect. It was concluded by McCrum et al that the β relaxation *is* the true glass transition.[148]

From the above information, it is still apparent that a debate remains among scientists regarding the relaxation (β or γ) attributable to the glass transition. However, both relaxations are below room temperature and thus deformation (stretching) of the film without the application of heat, i.e. stretching at room temperature, is possible. As mentioned above, the MEAUS process requires knowledge of T_g because stretching of the annealed film must occur above the T_g of the polymer for reasons now discussed.

2.4 Deformation of Lamellar Morphologies

The final stage of the MEAUS process is the stretching stage where the annealed planar stacked lamellar morphology is deformed parallel to the MD. Initial investigations of semicrystalline polymer deformation mechanisms largely focused on PE[149,150] and iPP[151,152].

From these studies, models were proposed to account for the mechanism of crystalline deformation. In general, the deformation mechanism can proceed via two pathways. The first is brittle fracture occurring under high loading rates at lower temperatures, and the second is ductile drawing after plastic deformation. The second deformation type occurs under lower rates of draw and higher temperature. Electron microscopy observations of the second deformation type done at room temperature on PE stacked lamellar morphologies where the draw direction was perpendicular to the stacked lamellae better elucidated the morphological response.[153] Initially, the response was amorphous interlayer deformation (i.e. between the stacked lamellae) with rigid separation (splaying) of the lamellae. As the tie-chains between the lamellae become taut, chain slip initiates within the crystalline lamellae. In addition, crystalline blocks shear apart with portions decrystallizing once they are below a critical crystal size.[153] With further draw, crystallization of the oriented amorphous regions occurs. [149-152]

In general, the predominant mode of crystal deformation is chain slip.[128] Lamellar shearing is also a relatively common process when deformation temperatures are above the glass transition of the polymer where lamellar shear occurs within the amorphous regions between adjacent lamellae.[154] In the case of the simple uniaxial deformation that occurs for the MEAUS process, chain slip and lamellar shear, do not account for the SAXS spacing increase observed for the stacked lamellae morphology upon draw. Thus a new deformation model, lamellar separation, was proposed[154] which *is* believed to be the deformation mode taken advantage of in the MEAUS method. The ability of the chains to translate through the crystalline lamellae (α_c relaxation) enables these types of semicrystalline polymers to be drawn to higher levels which thus allows greater lamellar separation.

In the case of ultradrawing, the ability of the chains to translate through the crystalline lamellae (α_c relaxation) enables these types of polymers to be drawn to higher extension levels. To prevent chain rupture, the chains must be pulled out of the crystals with energies below those

needed for rupture. A variety of other models have been proposed to account for ultradrawability. Aharoni[117] proposed thermal crystal transitions, Flory[155] suggested melting followed by recrystallization, Peterlin's[156] model, accounted for the phenomena by assuming a crystal axis rotation and axial shear. Schmidt et al. suggest that without the presence of the α_c relaxation (i.e. crystal mobility), as mentioned previously, the ability to ultra-draw is non-existent because chain translation through the crystal is not possible at energies below chain rupture. As shown in Figure 2.17, ultradrawable polymers versus non-ultradrawable are listed, and if the polymer possesses the ability for chain translation through the crystalline phase (α_c relaxation).

This above section now completes the discussion of the various stages of the uniaxial-stretching process and the mechanisms involved in these stages. The information covered is by no means all encompassing of that available regarding crystallization, melt-flow, annealing, and deformation. However, the discussion has provided the reader with an adequate understanding of the generalities involved in the MEAUS process. Two semicrystalline polymers, PMP and POM, were also introduced and discussed with regard to their relaxations. Further information will now be provided regarding other characteristics of these two polymers that is believed to be very relevant to this research proposal.

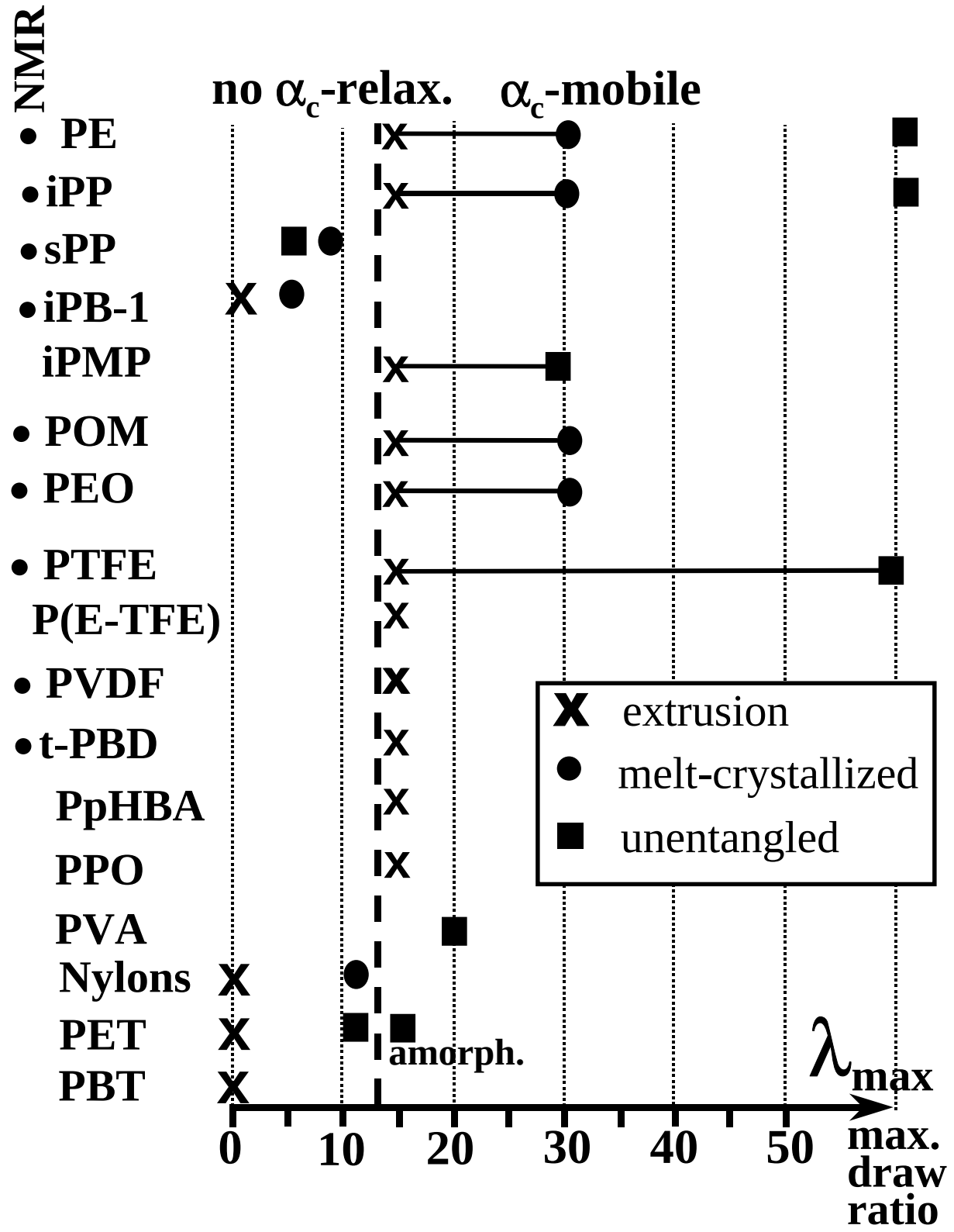

Figure 2.17 Semicrystalline polymers that possess and do not possess an α_c relaxation relative to their ability to ultradraw. Reproduced from K. Schmidt-Rohr.[157]

2.5 Poly(4-methyl-1-pentene) Morphological Characteristics

2.5-1 PMP Unit Cell:

Isotactic poly(4-methyl-1-pentene) is known to crystallize into more than one type of unit cell i.e. it is polymorphic. Crystalline PMP was first described by Natta et al in 1955[158,159], but it was not until 1958 that Frank et al quantified the dimensions of the first type of unit cell, otherwise known as modification I. Simultaneously, they reported that PMP can produce similar chain folded crystals[160] as does PE as first published by Keller[161].

Modification I possesses a tetragonal unit cell with four chains passing through each of the unit cell corners, the conformation of each chain being a 7/2 helix with the axes of the helices parallel to the "c"-axis of the unit cell. The large side group, emanating from the main chain every second carbon atom, is the cause for such a large "sloppy" helix. Figure 1.18 displays a comparison of the trans-planar zigzag conformation of PE, the 3/1 helix of iPP, and the 7/2 helix of PMP modification I. The unit cell dimensions of modification I are "a" equals "b" which equals 18.66 Å and "c" equals 13.80 Å.[161-164] The four other crystalline unit cells for PMP are known as modifications II, III, IV, and V. However upon heat treatment, these crystal modifications transform into modification I.[165-168] Most importantly, modification I is the only crystal form that occurs from the melt.[162,164]

The density of the PMP crystal modification I has been calculated to be between 0.813 to 0.832 g/cm^3 with studies utilizing X-ray diffraction and dilatometry.[169-172] In addition, the crystalline density or specific volume of PMP within a certain range of temperatures, shown in Figure 2.19, is less than that of the amorphous phase. For example, the crystalline density is 0.828 g/cm^3 while the amorphous density equals 0.838 g/cm^3 at 25°C.[162] The dependence of the specific volume on temperature was measured by Griffith and Ranby[172] as shown in Figure 2.19-note the crossover point at approximately 50°C. The optical properties are also affected by temperature with a sign change in spherulitic birefringence occurring at ca. 50°C.[173]

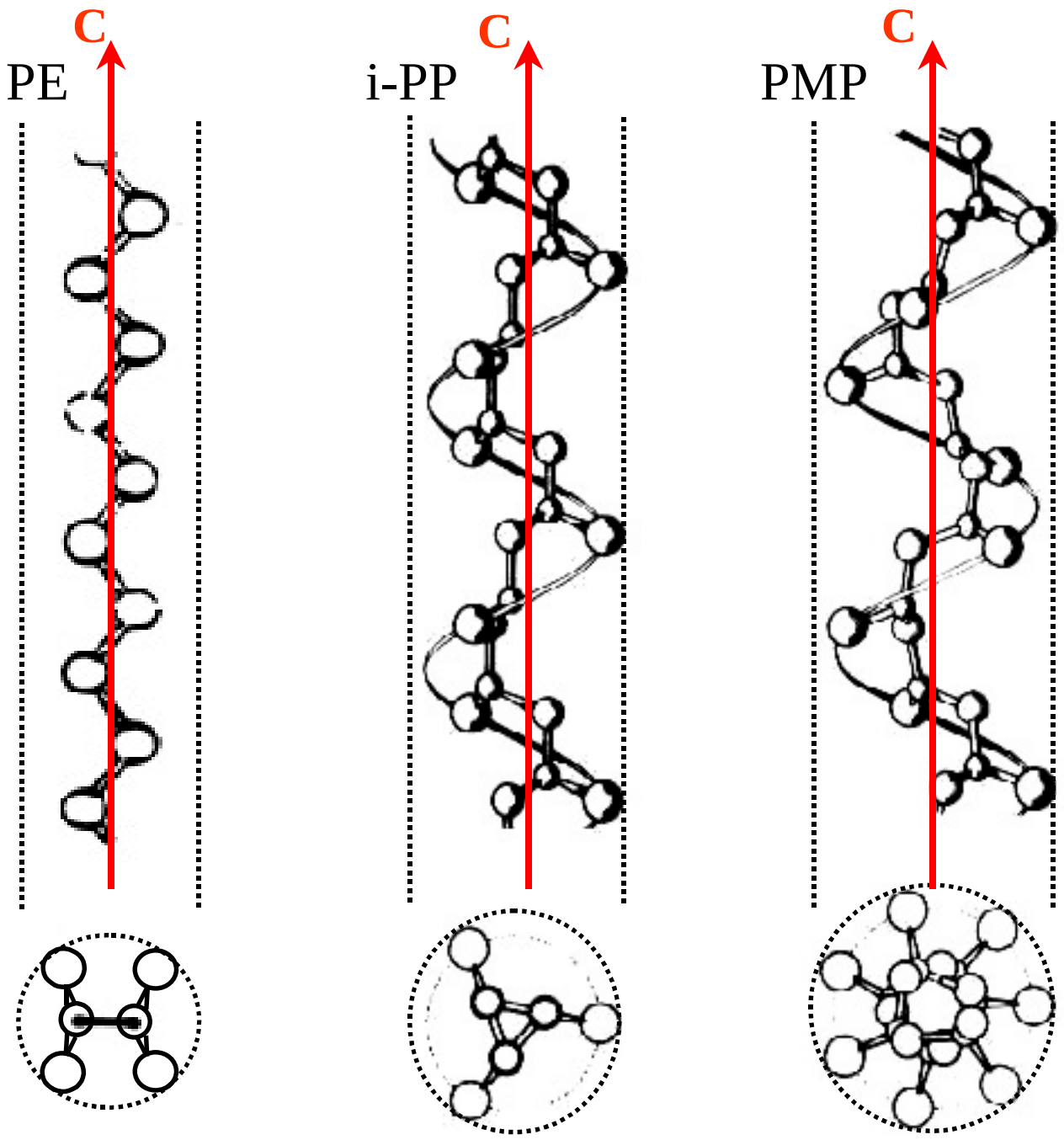

Figure 2.18 Chain length profile and cross-sections of the trans-planar zigzag conformation of PE, the 3/1 helical conformation of i-PP, and the 7/2 helical conformation of PMP.

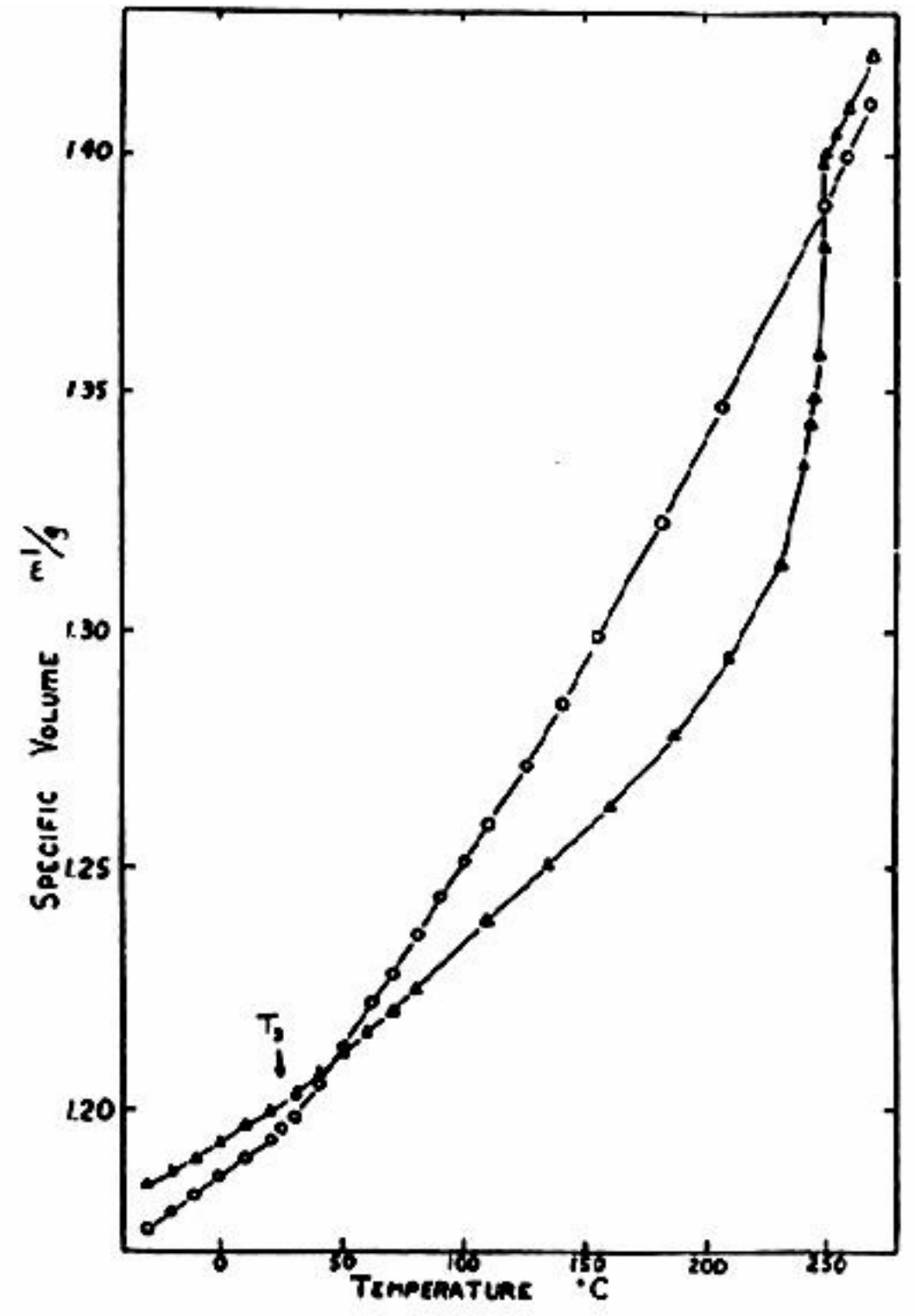

Figure 2.19 Specific volume dependence on temperature for crystalline and amorphous phases of PMP: (O) amorphous, (Δ) crystalline.[172]

2.5-2 Orientation Determination with emphasis on PMP:

The main reason for studying the rheo-optical properties of polymeric materials is to obtain information that aids in evaluating their molecular orientation and structure. Two of the main rheo-optical methods employed to obtain this information are linear dichroism and WAXS. The technique of linear dichroism can in some cases provide a quantitative measure of the orientation within a specific phase while WAXS can be used to determine the full distribution of chain orientations in the crystalline phase. In determining a quantitative value for orientation, the angular deviation of the average chain axis with respect to a specified reference axis is measured. A commonly reported parameter for uniaxially oriented systems that utilizes this angular deviation is a second moment average function, termed the Hermans' orientation, and is expressed by Eq 2.8.[174]

$$f_H = \frac{3\langle\cos^2\theta\rangle - 1}{2} \qquad \text{(Eq 2.8)}$$

The quantity $\langle\cos^2\theta\rangle$ represents the average value of $\cos^2\theta$ taken over all the polymer chains within the system or phase being measured. The value for θ is the angle between the average chain axis and the chosen reference axis. Hermans' function (f_H) has a maximum value of one ($f_H = 1$), when the average polymer chain is oriented parallel to that of the reference axis ($\theta = 0°$). The minimum of negative one half occurs when the average chain axis is oriented perpendicular to the reference axis (i.e. $\theta = 90°$ & $f_H = -1/2$). For random orientation, the value of f_H becomes zero and $\langle\cos^2\theta\rangle$ equals one third.

For extruded semicrystalline polymers, the degree of crystalline orientation (specifically the chain orientation within the crystalline phase) with respect to MD is of interest.[4,60,175] In general, the chain direction is defined along the c-axis of the unit cell thus the state of c-axis orientation is of importance. Figure 2.20 depicts the coordinate system used to define a tetragonal unit cell

with respect to a given set of orthogonal (x, y, z) axes. The angles α, β, and ε are measured with respect to the the z-axis (MD) and the a, b, and c crystallographic axes.

As discussed above, PMP possesses a tetragonal unit cell of dimensions a = b = 18.66 Å and c = 13.80 Å. Since a tetragonal unit cell possesses orthogonality, the law of cosines can be invoked:

$$\cos^2\alpha + \cos^2\beta + \cos^2\varepsilon = 1 \qquad \text{(Eq 2.9)}$$

If each of the axes (a, b, c) are defined in terms of its Hermans' orientation function, the following is obtained

$$f_a = \frac{3\langle\cos^2\alpha\rangle - 1}{2} \qquad \text{(Eq 2.10a)}$$

$$f_b = \frac{3\langle\cos^2\beta\rangle - 1}{2} \qquad \text{(Eq 2.10b)}$$

$$f_c = \frac{3\langle\cos^2\varepsilon\rangle - 1}{2} \qquad \text{(Eq 2.10c)}$$

upon combining Eqs 2.10 with Eq 2.9

$$f_a + f_b + f_c = 0 \qquad \text{(Eq 2.11)}$$

In the case of a tetragonal unit cell the "a"-axis equals the "b"-axis or f_a equals f_b ($\alpha = \beta$) thus,

$$2 \cdot f_a + f_c = 0 \qquad \text{(Eq 2.12)}$$

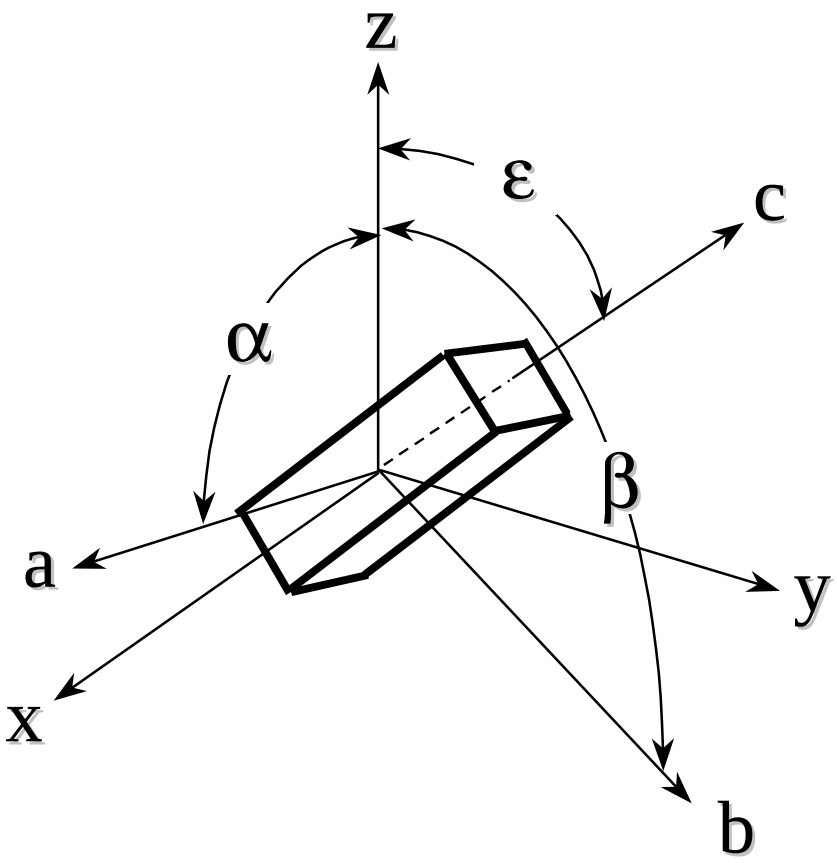

Figure 2.20 Coordinate system used to define the tetragonal unit cell with respect to a given set of orthogonal axes.

Hence, only a single reflection that is solely dependent on the "a"-axis (h00), "b"-axis (0k0), or "c"-axis (00l) is required to follow crystal orientation for a uniaxially oriented system. For uniaxially oriented PMP materials, the set-of-planes typically followed is the (200) set-of-planes.[9,175] Hermans' orientation function through trigonometric simplification becomes

$$f_{hkl} = \frac{3<\cos^2\theta_{hkl^*}\,\overline{\sin^2\Psi_{hkl}}> - 1}{2} \qquad \text{(Eq 2.13)}$$

The azimuthal dependence of the scattered intensity for an (hkl) reflection is defined by the angle Ψ_{hkl}, and the Bragg angle for the 200 (θ_{200}) is the angle between the center of the pattern, the center of the (200) scattering reflection, and the sample, as displayed in Figure 2.21a. A schematic depicting the azimuthal diffraction angle (Ψ_{200}) is shown in Figure 2.21b. The quantity $\sin^2\Psi_{hkl}$ is calculated by determining the scattering intensity of the appropriate scattering reflection as a function of angle. It is represented by the following relationship

$$\overline{\sin^2\psi_{200}} = \frac{\int_0^{\pi/2} I(\psi)\,\sin^2\psi_{200}\,\cos\theta_{200}\,d\psi}{\int_0^{\pi/2} I(\psi)\,\cos\theta_{200}\,d\psi} \qquad \text{(Eq 2.14)}$$

where $I(\psi_{200})$ is the relative intensity at the angle ψ_{200} for the (200) reflection. Equation 2.14 can also be evaluated graphically.[176-178] However, an approximation of $\sin^2\Psi_{hkl}$ can be obtained by measuring the half width of the appropriate (hkl) reflection.

As previously mentioned, another important technique often utilized to determine orientation is linear dichroism. This method is based upon selective absorption of polarized radiation by different chromophoric groups along the polymer chain. In addition, if a specific chromophore vibration is attributed to a specific phase, the orientation within that phase typically can be determined. Infrared (IR), visible, or ultraviolet electromagnetic radiation has been used for this

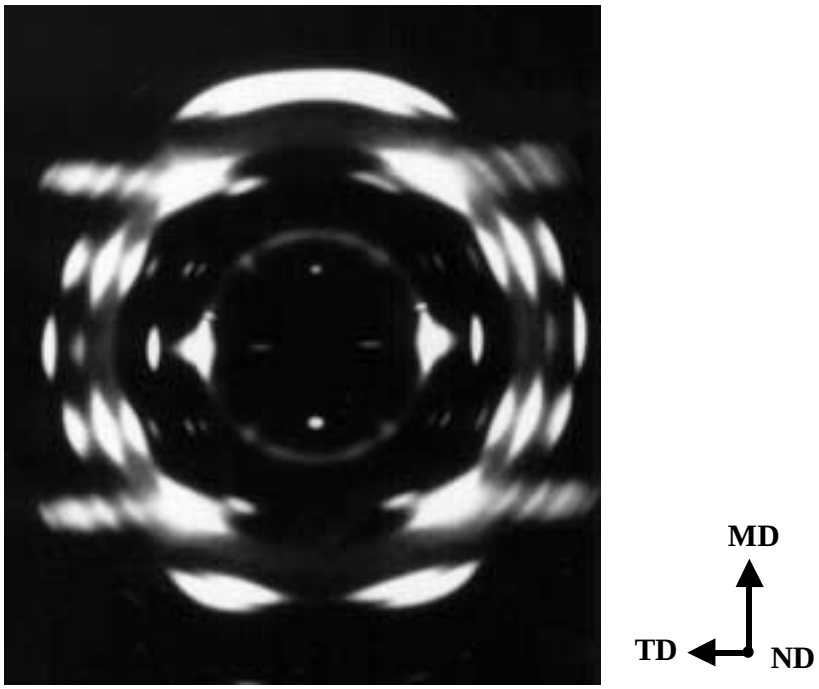

Figure 2.21a WAXS photograph of a melt extruded PMP precursor. MD direction shown.

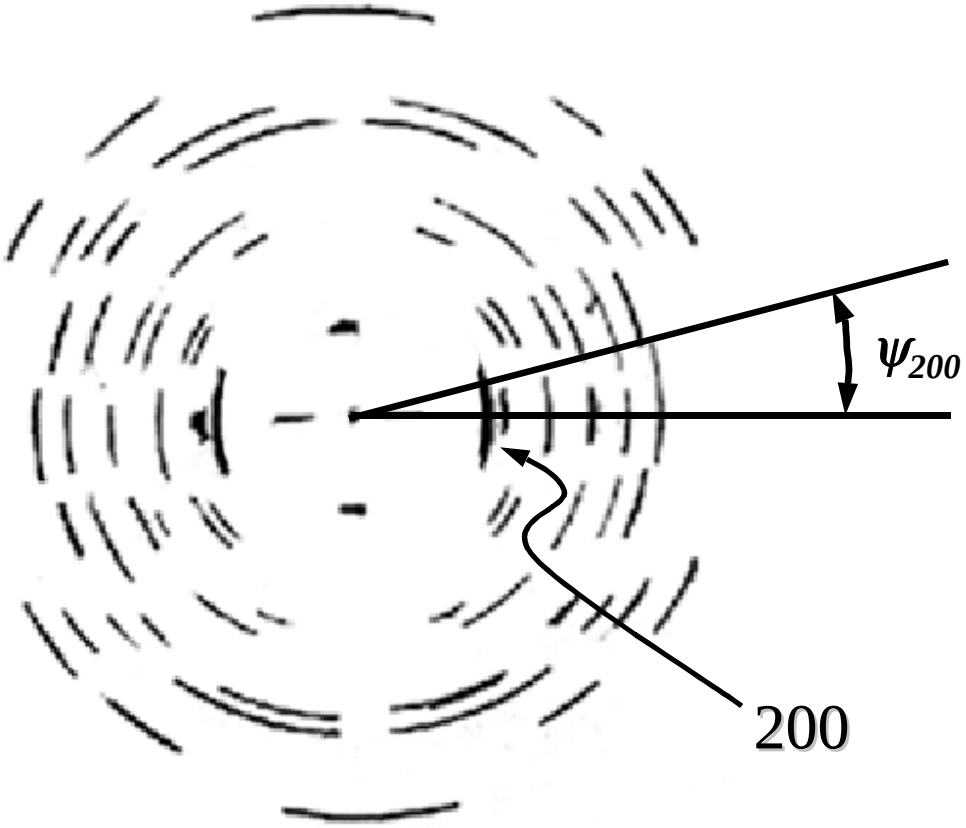

Figure 2.21b Schematic depicting the WAXS diffraction pattern for an oriented melt-extruded PMP film with the azimuthal diffraction angle (Ψ_{hkl}) for the (200) reflection defined.

technique. The selection of the type of radiation is based upon the chromophoric group to be analyzed. For most chromophoric groups of polymers, the frequencies absorbed are in the IR region, thus, Fourier Transform Infrared Spectroscopy (FTIR) is the main technique utilized.

If orientation exists, the absorption of plane-polarized radiation by a chromophoric group in two orthogonal directions, specifically parallel and perpendicular to a reference axis (MD), should be unequal with one exception noted below. The ratio of these two absorption values is defined as the dichroic ratio (D).

$$D = A_{II}/A_{\perp} \qquad \text{(Eq 2.15)}$$

Where A_{II} is the absorption parallel and $A_{\perp}$ is the absorption perpendicular to a specific reference axis. In general, three values of D exist with two being independent, but for uniaxial oriented systems only one value of D is required. This single dichroic ratio is related to the Hermans' orientation function by the following relationship

$$f_H = \left[\frac{(D_o + 2)}{(D_o - 1)}\right]\left[\frac{(D - 1)}{(D + 2)}\right] \qquad \text{(Eq 2.16)}$$

where $D_o = 2\cot^2\alpha$, and the value for α is the angle between the chromophore transition moment and the chain axis. Particular α values of interest are with respect to the possible extremes and when it equals 54.7degrees. When the transition moment is parallel with the chain axis, α takes on the value of zero and the first term in brackets of Eq 2.16 equals unity thus simplifying the equation. At the other extreme, when α equals 90 degrees, D_o equals zero, and the left-hand side of Eq 2.16 becomes a value of negative two. The case in which α equals 54.7 degrees results in a constant dichroic ratio of one (D =1) implying that there is a lack of preferential orientation inherent to the sample, even if orientation does exist.

The parameters required for determining f_H of Eq 2.16 are a known chromophoric vibration, the corresponding transition moment angle (α), and the ability to detect the resulting absorption. The amount of absorption is also a function of sample thickness.[174] For PMP, a vibration

specific to a single phase is not known. He and Porter[179], however, used the 918 cm^{-1} band, a rocking mode vibration from two methyl groups[180], to follow the dichroic ratio as a function of extension. In addition, He et al used hydrostatic extrusion to obtain different degrees of crystalline orientation as measured via WAXS. The WAXS values for Hermans' orientation function increased with draw ratio until a maximum value ca. 1 was obtained at a draw ratio of 30. Similarly, the dichroic ratio followed an asymptotic behavior with draw, and the dichroic ratio approached a value slightly above 5 at the same draw ratio of 30.[179]

Another rheo-optical technique utilized to aid in the evaluation of sample orientation is birefringence (Δ). Birefringence is defined as the difference in refractive index between two mutually perpendicular axes, and it employs linearly polarized light.[174] The simple relation

$$\Delta = \Delta^{\circ} * f_H \qquad \text{(Eq 2.17)}$$

relates the birefringence to Hermans' orientation function, where Δ° is the intrinsic birefringence. Intrinsic birefringence is the birefringence value for a fully oriented component in a given phase (i.e. $f_H = 1$).[181] As with the other measures of orientation, three different values for birefringence exist with two being independent, but uniaxial systems have only one independent value. This technique produces a system average orientation compared with what WAXS or IR linear dichroism are capable of measuring. However, with the aid of another technique (e.g. WAXS or IR dichroism), crystalline or amorphous orientations can be calculated. This can be done if the total birefringence is assumed to be due to additive contributions within the sample. The equation that results is

$$\Delta = X_c * \Delta_c^{\circ} * f_c + (1 - X_c) * \Delta^{\circ}_{am} * f_{am} + \Delta_{form} + \Delta_{dist} \qquad \text{(Eq 2.18)}$$

where X_c is the volume fraction of crystal phase, Δ_c° is the intrinsic birefringence of the crystalline phase, f_c is the crystalline orientation, Δ°_{am} is the amorphous phase intrinsic birefringence, f_{am} is the orientation of the amorphous phase, Δ_{form} is the form birefringence, and

Δ_{dist} is the distortional birefringence. The distortional birefringence or sometimes termed "glassy" birefringence can be neglected if the measurement is carried out above the polymer T_g. In contrast, form birefringence is due to a distortion of the incident light wave at an interface caused by two components possessing different refractive indices. In addition, one of the components must be geometrically anisotropic (i.e. non spherical), packed in some regular order, and of appropriate size (~ $\lambda/20$). Two examples include microporous materials or anisotropic stacked lamellae[181].

In addition to previously mentioned rheo-optical techniques, two others, SAXS and SALS, have potential use in the study of orientation and structure. Even though the radiation utilized by these two techniques is different, the physics of their scattering of the radiation remains the same. Specifically, the total scattered intensity (I_s) is dependent upon the difference between the scattering power of the particle and its surroundings to the second power, i.e. $I_s \propto (\rho_{xtal} - \rho_{amor})^2$ where $(\rho_{xtal} - \rho_{amor})$ is termed the contrast factor. For SAXS investigations of semicrystalline materials, $(\rho_{xtal} - \rho_{amor})$ is the difference between the crystalline and amorphous phase electron density. For PMP, the $(\rho_{xtal} - \rho_{amor})$ is insufficient at those temperatures shown in Figure 1.19 to obtain measurable SAXS intensity because of the similarity in density between the crystal and amorphous phases. As a solution to this dilemma, Tanigami and Miyasaka increased the temperature of the sample thereby increasing the density difference between phases and thus the contrast factor is increased. They found that at approximately 135°C sufficient contrast exists to observe significant SAXS scattering.[182] Another solution, as shown by Mizuno et al., was to increase the electron density of the amorphous phase by selectively staining it using a high vapor pressure solvent possessing a double bond (e.g. 1-dodecene). The samples were then vapor stained using OsO_4 which reacts with the double bonds of the high vapor pressure solvent via oxidation.[183] In addition, scattering experiments performed at sufficiently low temperatures,

where a significant contrast between the amorphous and crystalline phases does exists, would also present an alternative solution.

As occurs for SAXS at room temperature, a similar problem exists for SALS of PMP materials due to the lack of a significant contrast factor(s). In the case of SALS, the contrast factors are a function of the refractive indices of the polymer. For anisotropic scattering, H_v, the contrast factor is dependent upon the directionality of the spherulitic refractive indices, precisely the difference between the refractive indices parallel and tangential to the spherulitic radial direction i.e. $(n_r - n_t)$. As for isotropic scatter, V_v, the dependence is not only due to orientation considerations, $(n_r - n_t)$, but also due to density fluctuations between the crystalline and amorphous phases, $(n_{xtal} - n_{amor})$. As previously addressed for PMP at room temperature, there is little difference in density between the crystalline and amorphous phases thereby $(n_{xtal} - n_{amor})$ becomes insignificant. In addition, there is little directional dependence of the spherulitic refractive indices at room temperature and thus the difference between the two mutually perpendicular refractive indices, $(n_r - n_t)$, is inadequate. This inadequacy stems from the large side group emanating from the main chain every second carbon atom.[9,173] As a result light scattering of PMP specimens will not yield measurable scattering intensities at or near room temperature. However, light scattering, specifically H_v, does become measurable via optical microscopy utilizing crossed polarizers at or below –10°C disappearing until above 50°C and reaching a maximum at 225°C followed by complete loss at 245°C which is associated with the crystal phase melting.[173]

2.6 Morphological Characteristics of Polyoxymethylene

2.6-1 POM Unit Cell:

The unit cell of POM was first determined by Huggins[184] to be a 9/5 helical conformation and later substantiated by Tadokoro et al.[185]. Tadokoro et al also determined the unit cell geometry to

be trigonal (or hexagonal), and the lattice dimensions to be "a" equal to 4.47Å and "c" equals 17.39Å.[185] This was in conflict with earlier observations by Hengstenberg[186] and Sauter[187], who calculated the unit cell to be trigonal but with the lattice dimensions "a" equal to 4.46Å, "c" equal to 17.35Å and a 9/4 helical conformation. In addition, Hengstenberg[186] and Sauter[188] determined the unit cell to be composed of a single POM helix. Tadokoro also correctly observed that the unit cell is made up of a single POM helix that can possess either right-handed or left-handed character as long as all surrounding helices are of the same "handedness".[185] In addition to the observations of Tadokoro et al, an additional crystalline packing geometry, determined to be metastable, was observed by Carazzolo et al[189-191], making POM polymorphic. Sorensen et al. calculated this second packing geometry to be orthorhombic of the dimensions "a" equal to 7.65 Å, "b" equals 4.77 Å, and "c" equals 3.56 Å. In this metastable orthorhombic geometry, the POM chain rotates two units for a single helical turn (i.e. 2/1 helix),[192] and the unit cell is composed of two helices.[189] Experimentally at room temperature, the hexagonal morphology is the more stable form.[193] However, if the orthorhombic unit cell makes-up the initial crystalline morphology, through heating the hexagonal morphology is attained.[194] The reported density for the hexagonal unit cell ranges from 1.491 to 1.506 g/cm^3 [185,195-197] while for the metastable orthorhombic geometry the values are 1.501 to 1.533 g/cm^3 [197,198]. The amorphous density is reportedly between 1.21 to 1.25 g/cm^3.[184,195] Note that the crystalline density of POM is larger than that of the amorphous phase at all temperatures unlike PMP.

2.6-2 POM Orientation Determination:

Similar techniques for orientation determination are used on POM materials as were described above for PMP. There are differences in the application of the techniques with respect to POM versus PMP, and these differences stem from the different chemical and packing geometry's that lead to different physical characteristics. The main rheo-optical technique

employed for determining the crystalline orientation of POM has been WAXS.[10-14,199-202] In a similar way as was discussed for the tetragonal unit cell geometry of PMP, if dealing with a orthogonal packing geometry where the system possesses only uniaxial orientation, the law of cosines applies. Another similarity between the tetragonal unit cell of PMP and the hexagonal unit cell of POM is that both possess only two dimensions that are of different lengths (i.e. a & c) and thus Eq 2.12 applies. As a result, only a single scattering reflection dependent upon the "a"-axis, (h00), is sufficient to measure the main chain crystal orientation for POM uniaxially oriented systems. The set of (hkl) planes typically followed for POM materials are the (100) planes,[11-14] and a similar procedure as outlined in section 2.5-2 is used to evaluate the azimuthal dependence and Bragg angle of the (100) diffraction arc. Figures 2.22a and 2.22b display a POM WAXS pattern of a uniaxially oriented sample and a schematic of the pattern, respectively. The azimuthal diffraction angle, Ψ_{100}, corresponding to the (100) set of planes is also defined in Figure 2.22b.

Besides the similarities between PMP and POM with respect to WAXS analysis, the general orientation equations for linear dichroism studies on POM are the same as were outlined in section 2.5-2. However, there have been no published studies utilizing linear dichroism on POM materials. POM infrared spectra were first successfully analyzed by Novak[203] and Tadokoro[204,205]. From these studies, the 1235 cm^{-1} band was assigned to the crystal phase This band, however, is attributed to a complicated group of bond vibrations (rocking CH_2, 50%; bending C-O-C, 25%; symmetric stretching C-O-C, 24%).[205] As a result, there is no specific transition moment angle, α, that can be utilized to calculate D_o and thus only the dichroic ratio can be evaluated.

In addition to WAXS and linear dichroism, SAXS and light scattering analysis can be utilized for the study of POM. Birefringence has also been employed for rheo-optical studies of POM materials. For example, Zihlif[206] utilized birefringence on solid state extruded POM rods to

follow the sample orientation as a function of draw ratio to determine the intrinsic birefringence of POM. Further, Takeuchi et al.[207,208] applied a microwave heating and drawing technique to obtain highly oriented POM rods to also determine the intrinsic birefringence of POM. Takeuchi et al. claims to obtain a maximum crystalline orientation of 0.99, as measured via WAXS patterns, and the birefringence values corresponding to these samples were in the range of 0.078 to 0.08.[207,208] The birefringence values as measured by Zihlif follow the same pattern as those of Takeuchi et al. asymptotically increasing to ca 0.08 at nearly the same level of extension as Takeuchi et al.[206] From these studies, both authors concluded the intrinsic birefringence to be in the range of 0.078 to 0.080.

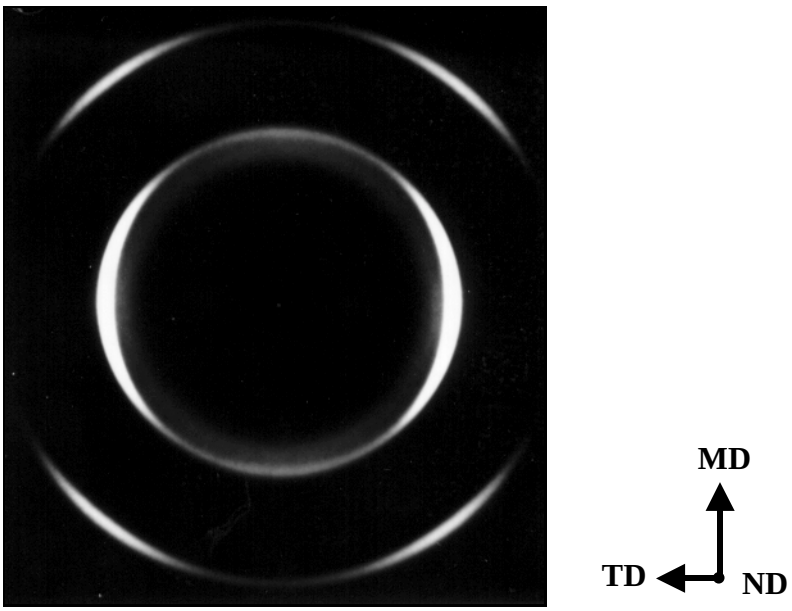

Figure 2.22a WAXS photograph of POM precursor. Note the indication of "a"-axis orientation in the meridonal region of the (100) scattering reflection. The MD direction is shown.

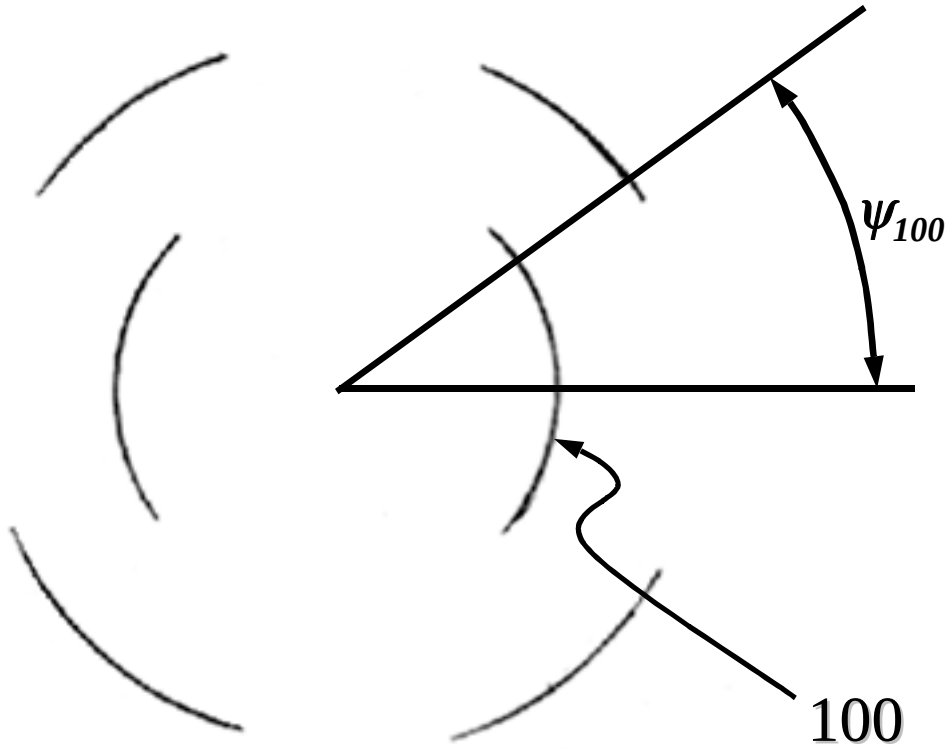

Figure 2.22b Schematic depicting the WAXS diffraction pattern for an oriented melt-extruded POM film with the azimuthal diffraction angle (Ψ_{hkl}) for the (100) reflection defined.

References

[1] Cannon, S. L., Mckenna, G. B., Statton, W. O., *J. Polymer Sci., Macromol. Rev.*, 11, 209, (1976).
[2] Sprague, B. S., *J. Macromol. Sci.-Phys.*, B8(1), 157, (1973).
[3] Noether, H. D., Whitney, W., *Kolloid-Z.U.Z. Polym.*, 251, 991, (1973).
[4] Yu, T. H., Ph.D. Dissertation (advisor: G. L. Wilkes) Virginia Tech, 1995.
[5] Kamo, J., Uchida, M., Hirai, T., Japanese patent 63[1988]-256712, 1988.
[6] Twarowska-Schmidt, K., Wlochowicz, A., *J. Membrane Sci.*, 137, 55, (1997).
[7] Aharoni, S. M., Sibilia, J. *P., Polym. Eng. Sci.*, 19(6), 450, (1979).
[8] Pennings, A. J., Smook, J., de Boer, J., Gogolewski, S., van Hutten, P. F., *Pure Appl. Chem.*, 55, 777, (1983).
[9] Choi, C. H., White, J. L., Intern. Polym. Processing: Fibers and Films, Hanser Publishers, Munich, 1998.
[10] Geil, P. H., "Polymer Single Crystals," Interscience, New York, 1963.
[11] Enns, J. B., Simha, R., *J. Macromol. Sci.-Phys.*, B13, 25, (1977).
[12] Bigg, D. M., *Polym. Eng. Sci.*, 28(13), 830, (1988).
[13] Nakagawa, K., Yamamoto, F., Takeuchi, Y., Yamakawa, S., *J. Polym. Sci.: Polym. Phys. Ed.*, 23, 1193, (1985).
[14] Garber, C., Clark, E., *J. Macromol. Sci., Phys.*, 4, 499, (1970).
[15]Strathmann, H., "Synthetic Membranes: Science, Engineering, and Applications", ed. P. M. Bungay, H. K. Lonsdale, M. N. de Pinho, Riedel Publishing, New York, 1983.
[16] Turbak, A. F., Synthetic Membranes, 2, ACS Symposium Series No. 154, (1981).
[17] Yamashita, A., Kawai, S., Tanii, K., & Takakura, K., US patent 4,269,713, 1981.
[18] Hamilton, R., Ford, C., Colton, C., Cross, R., Steinmuller, S., Henderson, L., *Trans. Am. Soc. Artif. Intern. Organs.*, 17, 259, (1971).
[19] Bixler, H. J., Nelsen, L. M., Bluemle, L. W., *Trans. Am. Soc. Artif. Intern. Organs.*, 14, 99, (1968).
[20] Henderson, L. W., Colton, C. K., Ford, C. A., *J. Lab. Clin. Med.*, 85(3), 372, (1975).
[21] Harper, B. G., *J. Appl. Polym. Sci.*, 1959, 1 (1), 50.
[22] Takita, K., Kono, K., Takashima, T., Okamota, K., US patent 5,051,183, 1991.
[23] Rein, D., H., Baddour, R. F., Cohen, R. E., *J. Polym. Eng.*, 12(4), 353, (1993).
[24] Fleischner, R. L., Price, P. B., Walker, R. M., *Sci. Amer.*, 220, 30, (1969).
[25] Leob, et al., US patent 3,133,132, 1964.
[26] Rein, D. H., Baddour, R. F., Cohen, R. E., *J. Polym. Eng.*, 12(4), 353, (1993).
[27] Williams, J. L., Gunther, H., Peterlin, A., US patent 89,516, 1974.

[28] Soehngen, J., Ostrander, K., US patent 4,257,997, (1981); assigned to Celanese Corp.
[29] Nago, S., Mizutani, Y., *J. Appl. Polym. Sci.*, 68, 1543, (1998).
[30] Mizutani, Y., Nakamura, S., Kaneko, S., and Okamura, K., *Ind Eng. Chem. Res.*, 32(1), 221, (1993).
[31] Nakamura, S., Okamura, K., Kaneko, S., Mizutani, Y., J. Appl. Polym. Sci., 49, 143, (1995).
[32] Morosff, N., Peterlin, A., *J. Polym. Sci., Part A-2*, 10, 1237, (1972).
[33] Machin, M. J., Keller, A., *J. Macromol. Sci.*, B1(1), 41, (1967).
[34] Celanese Corp. of America, Belgian patent 650,890, 1965.
[35] Herrman, A. J., US patent 3,256,258, 1966, assigned to E. I. Du Pont de Nemours and Co. Inc.
[36] Garber, C. A., Clark, E. S., *J. Macromol. Sci.-Phys.*, B4(3), 499, (1970); *Int. J. Polym. Mater.* 1, 31, (1971).
[37] Hashimoto, T., Todo, A., Murakami, Y., *J. Polym. Sci. Polym. Phys. Ed.*, 15, 501, (1977).
[38] Knobloch, F. W., Statton, W. O., US Patent 3,299,171, 1967, assigned to E. I. Du Pont de Nemours and Co. Inc.
[39] Quynn, R. G., Brody, H., *J. Macromol. Sci.-Phys.*, B5(4), 721, (1971).
[40] Tanhigami, T., Yamaura, K., Matsuzawa, S., *J. Appl. Polym. Sci.*, 32, 4491, (1986).
[41] Druin, M. L., Loft, J. T., Plovan, S. G., US patent 3,801,404, 1974, assigned to Celanese Corp.
[42] Mansfield, M., Boyd, R., *J. Polym. Sci., Phys. Ed.*, 16, 1227, (1978).
[43] Adams, W. W., Yang, D., Thomas, E. L., *J. Mater. Sci.*, 21, 2239, (1986).
[44] Quynn, R. G., Sprague, B. S., *J. Polym. Sci.*, 8, A-2, 1971, (1970).
[45] Ward, I. M., "An Introduction to the Mechanical Properties of Solid Polymers", John Wiley & Sons Inc., 1993.
[46] Noether, H. D., US Patent 3,513,100, 1970, Celanese Research Corp.
[47] Gore, R. W., US Patent 39,621,253, 1967.
[48] Chen, R. T., Saw, C. K., Jamieson, M. G., Aversa, T. R., Callahan, R. W., *J. Appl. Polym. Sci.*, 53, 471, (1994).
[49] Hoffman, J. D., Davis, T., Lauritzen Jr., J. I., "Treatise on Solid State Chemistry," Vol. 3, Editor: N. B. Hannay, Plenum Press, New York, 1976.
[50] Keller, A., Kolnaar, H., "Materials Science and Technology A Comprehensive Treatment", Chpt 4, 18, pg 189-268, John Wiley and Sons, 1997.
[51] Hikosaka, M, Ghosh, S. K., Toda, A, *ACS PMSE Proceedings*, 81, 332, (1999).
[52] Wunderlich, B., "Macromolecular Physics", Academic Press, New York, 1976.
[53] Alfonso, G. C., *ACS PMSE Proceedings*, 81, 330, (1999).
[54] Misra, A., Stein, R. S., Chu, C., Desai, A. B., Wilkes, G. L., *Polymer Lett. Ed.*, 13, 303, (1975).
[55] Mohajer, Y., Wilkes, G. L., Orler, B., *Polym. Eng. Sci.*, 24(5), 319, (1984).
[56] Pogodina, N., Winter, H., *Macromolecules*, 31, 8164, (1998).

[57] Pogodina, N., Winter, H., Srinivas, S., *ACS PMSE Proceedings*, 81, 246, (1999).
[58] Peterlin, A., *J. Macromol. Sci.-Phys.*, B7(4), 705, (1973).
[59] Mackley, M. R., Keller, A., *Phil. Trans., Lond.*, 278, 4, (1976).
[60] Zhou, H., Wilkes, G. L., *J. Mater. Sci.*, 33, 287, (1998).
[61] Clark, E. S., Scott, L. S., *Polym. Eng. Sci.*, 14(10), 682, (1974).
[62] Capaccio, G., Ward, I. M., *Polymer*, 15, 233, (1974).
[63] Porter, R. S., Wang, L., *J. M. S.-Rev. Macromol. Chem. Phys.*, C35(1), 63, (1995).
[64] Keller, A., Kolnaar, J. W. H., *Progr. Colloid Polym. Sci.*, 92, 81, (1993).
[65] Pennings, A. J., Kiel, A. M., *Kolloid-Z.*, 205, 160, (1965).
[66] Wikjord, A. G., Manley, J., *J. Macromol. Sci.-Phys.*, B4, 397, (1970).
[67] McHugh, A. J., Blunk, R. H., *Macromolecules*, 3, 261, (1970).
[68] Pennings, A. J., J. Polym. Sci., C16, 1799, (1967).
[69] Kobayashi, E., Okamura, S., Signer, R., *J. Appl. Polym. Sci.*, 12, 1661, (1968).
[70] Pennings, A. J., van der Mark, J. M. A. A., Booij, H. G., *Kolloid Z. u. Z. Polymere*, 236, 99, (1970).
[71] Taylor, G. I., *Proc. R. Soc. Lond.*, A 146, 501, (1934).
[72] Pennings, A. J., van der Mark, J. M. A. A., Kiel, A. M., *Kolloid Z. u. Z. Polymere*, 237, 336, (1970).
[73] Ziabicki, A., *J. Appl. Polym. Sci.*, 11(4), 14, (1959).
[74] Peterlin, A., *J. Polym. Sci.*, B4, 287, (1966).
[75] Frank, F. C., *Proc. R. Soc. Lond.*, A 319, 127, (1970).
[76] Keller, A., *J. Polym. Sci.*, 15, 31, (1955).
[77] Yeh, G. S. Y., Hong, H. Z., *Polym. Eng. Sci.*, 19(6), 395, (1979).
[78] Hoffman, J. D., Miller, R. L., *Polymer*, 38, 3151, (1997).
[79] Nagasawa, T., Matsumura, T., Hoshino, S., *Appl. Polym. Symp.*, 20, 295, (1973).
[80] Keller, A., Personal communication
[81] Cheng, S. Personal communication
[82] Geil, P., personal communication
[83] de Gennes, P. G., *J. Chem. Phys.*, 60, 15, 1974.
[84] Bayer, R. K., Michler, G. H., Balta-Calleja, F. J., *PMSE Vol. 81*, Fall, 1999.
[85] Edwards, S. F., *Polymer*, 9, 140, (1977).
[86] Keller, A., Kolnaar, H., "Materials Science and Technology A Comprehensive Treatment", Chpt 4, 18, pg 189-268, John Wiley and Sons, 1997.
[87] Odell, J. A., Keller, A., Muller, A. J., *Colloid Polym. Sci.*, 263, 181, (1985).
[88] Odell, J. A., Keller, A., Muller, A. J., *Colloid Polym. Sci.*, 270, 307, (1992).
[89] Janzen, J., Rohlfing, D. C., Hicks, M., *J. Rheol.*, submitted 1997.
[90] Jordens, K., private communication
[91] Graessley, W. W., *J. Chem. Phys.*, 47(6), 1942, (1967); *Adv. Polym. Sci.*, 16, 1, (1974).

[92] Cox, W. P., Merz, E. H., *J. Polym. Sci.*, 28, 619, (1958).
[93] Gupta, A., Simpson, D., Harrison, I., *J. Appl. Polym. Sci.*, 50, 2085 (1993).
[94] Pazur, R., Prud'homme, R., *Macromolecules*, 29, 119, (1996).
[95] Zhou, H., Wilkes, G. L., *Polymer*, 38(23), 5735, (1997).
[96] Butler, M., Donald, A., *J. Appl. Polym. Sci.*, 67, 321, (1998).
[97] Choi, K., Spruiell, J., White, J., *J. Polym. Sci.: Polym. Phys. Ed.*, 20, 27, (1982).
[98] Hong, K., Spruiell, J., *J. Appl. Polym. Sci.*, 30, 3163, (1985).
[99] Shimomura, Y., Spruiell, J., White, J., *J. Appl. Polym. Sci.*, 27, 2663, (1982).
[100] Maddams, W., Preedy, J., *J. Appl. Polym. Sci.*, 22, 2721, (1978).; J. Appl. Polym. Sci., 22, 2739, (1978); *J. Appl. Polym. Sci.*, 22, 2751, (1978).
[101] Choi, K., Spruiell, J., White, J., *J. Appl. Polym. Sci.*, 25, 2777, (1980).
[102] McRae, M., Maddams, W., *J. Appl. Polym. Sci.*, 22, 2768, (1978).
[103] Huck, N., Clegg, P., *SPE Trans.*, 121, July, (1961).
[104] Stehling, F., Speed, C., Westerman, L., *Macromolecules*, 14, 698, (1981).
[105] White, J., Matsukura, Y., Kang, H., Yamane, H., Intern. Polym. Processing, 1, 83, (1987).
[106] Sheehan, W. C., Cole, T. B., *J. Appl. Polym. Sci.*, 8, 2359, (1964).
[107] Spruiell, J. E., White, J. L., *Polym. Eng. Sci.*, 15, 660, (1975).
[108] Jinan, C., Kikutani, T., Takaku, A., Shimizu, J., *J. Appl. Polym. Sci.*, 37, 2683, (1989).
[109] Stehling, F., Speed, C., Westerman, L., Macromol., 14, 698, (1981).
[110] Manzione, L., Jameel, H., Wilkes, G. L., *J. Polym. Sci.: Polym. Lett.*, 16, 237, (1978).
[111] Yeh, G. S. Y., Hosemann, R., Loboda-Cakovic, J., Cackovic, H., *Polymer*, 17, 309, (1976).
[112] Wunderlich, B., Macromolecular Physics, Academic Press, New York, 1973.
[113] Boyd, R. H., *Polymer*, 26, 323, (1985).
[114] Boyd, R. H., *Polymer*, 26, 1123, (1985).
[115] Enns, J., Simha, R., *J. Macromol. Sci.-Phys.*, B13, 11, (1977).
[116] Tormala, P., *J. Macromol. Rev. Macromol. Chem.*, C17, 297, (1970).
[117] Tanhigami, T., Yamaura, K., Matsuzawa, S., *J. Appl. Polym. Sci.*, 32, 4491, 1986.
[118] Gore, R. W., U. S. Patent 39,621,253, 1967.
[119] Rault, J., J.M.S.- Rev. Macromol. Chem. Phys., C37(2), 335, (1997).
[120] Hoffman, J. D., Williams, G., Passaglia, E., *J. Polym. Sci., Part C*, 14, 173, (1966).
[121] McCrum, N. G., Read, B. E., Williams, G., Anelastic and Dielectric Effects in Polymeric Solids, Wiley, New York, 1967.
[122] Hedvig, P., Dielectric Spectroscopy of Polymers, A. Hilger, Bristol, 1977.
[123] Boyd, R. H., *Macromolecules*, 25, 323, (1984).
[124] Gibson, A. G., Davies, G., Ward, I. M., *Polymer*, 19, 683, (1978).
[125] Garrett, P., Grubb, D., *J. Polym. Sci.: Part B: Polym. Phys.*, 26, 2509, (1988).

[126] Ohta, Y., Yasuda, H., *J. Polym. Sci.: Part B: Polym. Phys.*, 32, 2241, (1994).
[127] Aharoni, S. M., Sibilia, J. P., *Polym. Eng. Sci.*, 19, 450, (1979).
[128] Porter, R. S., Wang, L., *J. Macromol. Sci., Rev. Macromol. Chem. Phys.*, C35(1), 63, (1995).
[129] Uehara, H., et al., *Polym. Journal*, 29, 198, (1997).
[130] Woodward, A. E., Sauer, J. A., Wall, R. A., J. Polym. Sci., 117, (1961).
[131] Reddy, S., Desai, P., Abhiraman, A. S., Beckman, H. W., et al., *Macromolecules*, 30, 3293, (1997).
[132] Penn, R. W., *J. Polym. Sci. Part A-2*, 4, 559, (1966).
[133] Popli, R., Glotin, M., Mandelkern, L., J. Polym. Sci., Phys., 22, 407, (1984).
[134] Schmidt-Rohr, K., Personal communication
[135] Williams, G., *Polymer*, 4, 27, (1963).
[136] Ishida, Y., et al., *Kolloid Z.*, 174, 124, (1961).
[137] Thurn, H., *Kolloid Z.*, 173, 72, (1960).
[138] Read, B. E., Williams, G., *Polymer*, 2, 239, (1961).
[139] McCrum N. G., *J. Polym. Sci.*, 54, 561, (1961).
[140] Takayanagi, M., *High Polymers*, 10, 289, (1961).
[141] Eby, R. K., *J. Chem. Phys.*, 37, 2785, (1963).
[142] Arisawa, K., Tsuge, K., Wada, Y., *Rept. Progr. Polymer Phys.* (Japan), 6, 151, (1963).
[143] Wetton, R. E., Allen, G., *Polymer*, 7, 331, (1966).
[144] Bohn, L., *Kolloid Z.*, 201, 20, (1965).
[145] Keating, M. Y., Sauer, B. B., Flexman, E. A., *J. Macromol. Sci.-Phys.*, B36(6), 717, (1997).
[146] McCrum, N. G., Read, B. E., Williams, G., Anelastic and Dielectric Effects in Polymeric Solids, Dover, New York, 1967, pgs. 540-551.
[147] Kazen M. E., Geil, P. H., *J. Macromol. Sci.-Phys.*, B13, 381, (1977).
[148] McCrum, N. G., *J. Polym. Sci.*, 54, 561, (1961).
[149] Peterlin, A., Sakaoku, K., *J. Appl. Phys.*, 38, 4152, (1967).
[150] Sakaoku, K., Peterlin, A., *J. Macromol Sci. Phys.*, 1, 401, (1967).
[151] Sakaoku, K., Peterlin, A., *J. Polym. Sci.*, Part A-2, 9, 895, (1971).
[152] Morosoff, N., Peterlin, A., *J. Polym. Sci.*, Part A-2, 10, 1237, (1972).
[153] Adams, W. W., Yang, D., Thomas, E. L., *J. Mater. Sci.*, 21, 2239, (1986).
[154] Pope, D. P., Keller, A., *J. Polym. Sci.*, 13, 533, (1975).
[155] Mandelkern, L., Fundamentals of Polymer Crystallization, McGraw-Hill, New York, 1964.
[156] Peterlin, A., *J. Macromol. Sci.-Phys.*, B7(4), 705, (1973).
[157] Schmidt-Rohr, K. Private Communication.
[158] Natta, G., Pino, P., Mazzanti, G., Corradini, P., Giannini, U., *R. C.. Accad. Naz. Lincei*, 19, 397, (1955).
[159] Natta, G., Corradini, P., Bassi, I. W., *R. C. Accad. Naz. Lincei*, 19, 404, (1955).
[160] Frank, F. C., Keller, A., O'Connor, A., *Philos. Mag.*, 4, 200, (1959).

[161] Keller, A., *Phil. Mag.*, 2, 1171, (1957).
[162] Litt, M., *J. Polym. Sci.*, Part A, 1, 2219, (1963).
[163] Zoller, P., *J. Appl. Polym. Sci.*, 21, 3129, (1977).
[164] Kusanagi, H., Takase, M., Chatani, Y., Takodoro, H., *J. Polym. Sci., Polym. Phys. Ed.*, 16, 131, (1978).
[165] Charlet, G., Delmas, G., et al., *Polymer*, 25, 1613, (1984).
[166] Charlet, G., Delmas, G., *Polym. Bull.*, 6, 367, (1982).
[167] Kissin, Y. V., Encyclopedia of Polymer Science and Engineering, Vol. 9, ed. Kroschwitz, J. I., Wiley, New York, 1987, p. 707.
[168] Hasegawa, R., Tanabe, Y., Kobayashi, M., Takodoro, H., Sawaoka, A, Kawai, N., *J. Polym. Sci.*, Part A-2, 8, 1073, (1970).
[169] Schaefgen, J. R., *J. Polym. Sci.*, 38, 549, (1959).
[170] Mandelkern, L., Fundamentals of Polymer Crystallization, McGraw-Hill, New York, 1964.
[171] Zoller, P., Starkweather Jr., H. W., Jones, G. A., *Ibid.*, 15, 2271, (1977).
[172] Griffith, J. H., Ranby, B. G., *J. Polym. Sci.*, 44, 369, (1960).
[173] Saunders, F. L., *J. Polym. Sci., Polym. Lett. Ed.*, 2, 755, (1964).
[174] Wilkes, G. L., Encycl. Polym. Sci. & Eng., John Wiley & Sons, Inc., 14, 542, (1988).
[175] Choi, C., White, J., *ANTEC preprints*, 228, 2011, (1997).
[176] Stein, R. S., Norris, F. H., *J. Polym. Sci.*, 21, 381, (1956).
[177] Stein, R. S., *J. Polym. Sci.*, 31, 327, (1958).
[178] Stein, R. S., *J. Polym. Sci.*, 31, 335, (1958).
[179] He, T., Porter, R. S., *Polymer*, 28, 946, (1987).
[180] Gabbay, S. M., Stivala, S. S., *Polymer*, 17, 121, (1976).
[181] Stein, R. S., Newer Methods in Polymer Characterization, Wiley & Sons-Interscience, New York, 1964.
[182] Tanigami, T., Miyasaka, K., *J. Polym. Sci., Polym. Phys. Ed.*, 19, 1865, (1981).
[183] Mizuno, A., Nakamoto, H., Kumura, N., Moritani, Y., *Polymer*, 33(10), 2229, (1992).
[184] Huggins, M. L., *J. Chem. Phys.*, 13, 37, (1945).
[185] Uchida, T., Tadokoro, H., *J. Polym. Sci.*, Part A-2, 5, 63, (1967).
[186] Hengstenberg, J., *Ann. Physik*, 86, 4948, (1927).
[187] Sauter, E., Z., *Physik. Chem.*, 21B, 186, (1933).
[188] Sauter, E., *Z. Physik. Chem.*, 21B, 186, (1933).
[189] Carazzolo, G. A., Mammi, M., *J. Polymer Sci.* A, 1, 965, (1963).
[190] Mortillario, L., Galliazzo, G., Bessi, S., *Chem. Ind.* (Milan), 46, 139, (1964).
[191] Iguchi, M., *Polymer*, 24, 915, (1983).
[192] Sorensen, R. L., Liau, W. B., Kesner, L., Boyd, R. H., *Macromolecules*, 21, 200, (1988).
[193] Boyd R. H., Advances in Polymer Science: Prediction of Polymer Crystal Structures and Properties, Vol. 116, Springer-Verlag, Berlin, 1994.

[194] Kobayashi, M., Morishita, H., Shimomura, M., Iguchi, M., *Macromolecules*, 20, 2453, (1987).
[195] Hammer, C. F., Koch, T. A., Whitney, J. F., *J. Appl. Polym. Sci.*, 1, 169, (1959).
[196] Sauter, E., Z. *Physik. Chem.*, B18, 818, (1932).
[197] Carazzolo, G., *J. Polym. Sci.* A, 1, 1573, (1963).
[198] Becker, L., Wiss., *Nature*., 11, 3, (1962).
[199] O'leary, K., Geil, P. H., *J. Macromol. Sci.-Phys*., B2(2), 261, (1968).
[200] Siegmann, A., Geil, P. H., *J. Macromol. Sci.-Phys*., B4(3), 557, (1970).
[201] Singhania, A. K., Geil, P. H., *Die Makromole. Chemie*, 143, 231, (1971).
[202] Nakamae, K., Nishino, T., Shimizu, Y., Hata, K., Polymer, 31, 1909, (1990).
[203] Novak, A., Whalley, E., *Trans. Faraday Soc.*, 55, 1484, (1959).
[204] Tadokoro, H., Yasumoto, T., Morimoto, G., Murahashi, S., *Chem. High Polymers* (Tokyo), 17, 95, (1960).
[205] Tadokoro, H. Kobayashi, A., Kawaguchi, Y., Sobajima, S., Murahashi, S., Matsui, Y., *J. Chem. Phys*., 35(1), 369, (1961).
[206] Zihlif, A. M., *Mat. Chem. Phys*., 13, 21, (1985).
[207] Takeuchi, Y., Nakagawa, K., Yamamoto, F., *Polymer*, 26, 1929, (1985).
[208] Takeuchi, Y., Yamamoto, F., Nakagawa, K., *J. Polym. Sci., Polym. Phys. Ed.*, 27, (1986).